DETECTING NEAR-EARTH OBJECTS USING CROSS-CORRELATION WITH A POINT SPREAD FUNCTION

THESIS

Anthony O'Dell, Captain, USAF

AFIT/GE/ENG/09-30

DEPARTMENT OF THE AIR FORCE
AIR UNIVERSITY

AIR FORCE INSTITUTE OF TECHNOLOGY

Wright-Patterson Air Force Base, Ohio

The views expressed in this thesis are those of the author and do not reflect the official policy or position of the United States Air Force, Department of Defense, or the U. S. Government.

AFIT/GE/ENG/09-30

DETECTING NEAR-EARTH OBJECTS USING CROSS-CORRELATION WITH A POINT SPREAD FUNCTION

THESIS

Presented to the Faculty

Department of Electrical and Computer Engineering
Graduate School of Engineering and Management

Air Force Institute of Technology

Air University

Air Education and Training Command

In Partial Fulfillment of the Requirements for the

Degree of Master of Science (in Electrical Engineering)

Anthony O'Dell, BSA

Captain, USAF

March 2009

AFIT/GE/ENG/09-30

DETECTING NEAR-EARTH OBJECTS USING CROSS-CORRELATION WITH A POINT SPREAD FUNCTION

Anthony O'Dell, BSA
Captain, USAF

Approved:

/signed/	16 Mar 09
Stephen C. Cain, GS-14, USAF (Chairman)	date
/signed/	16 Mar 09
Michael Hawks, Lt Col, USAF (Member)	date
/signed/	9 Mar 09
Adam MacDonald, Lt Col, USAF (Member)	date

Abstract

This thesis describes a process to help discover Near-Earth Objects (NEOs) of larger than 140 meters in diameter from ground based telescopes. The process involves using Nyquist sampling rate to take data from a ground-based telescope and measuring the atmospheric seeing parameter, r_0, at the time of data collection. r_0 is then used to create a point spread function (PSF) for a NEO at the visual magnitude limit of the telescope and exposure time. This PSF is cross-correlated with the Nyquist sampling rate image from the telescope to reduce the noise and therefore increase the detection probability of a faint NEO. The process is compared to the current detection technique of using Rayleigh sampling with a threshold detector. This process is tested versus improper seeing parameter measurement and different locations of the NEO within the charged-coupled device (CCD) pixel field of view (FOV). The biggest improvement is where the NEO is located in the corner of the pixel FOV. The new process shows improvement in detection probability over the current process in all simulations.

Acknowledgements

I would like to thank my family and friends for the support the guidance through the years that have brought to this point in my life. I would also like to thank Professor Stephen Cain for his time, guidance, and patience as this thesis evolved over time.

Anthony O'Dell

Table of Contents

Page

List of Figures

DETECTING NEAR-EARTH OBJECTS USING CROSS-CORRELATION WITH A POINT SPREAD FUNCTION

I. Introduction

1.1 General Issue

Near Earth Objects (NEOs) have been hazards for earth since its formation. It is theorized that a large NEO impact in the Yucatan Peninsula caused the extinction of the dinosaurs in the Cretaceous Period [Fix, 1995]. Even the Moon is pot marked by many impact craters and numerous craters can be found on the Earth's surface as evidence of more recent NEO impacts. Even NEOs that do not reach the Earth's surface can have dramatic effects on life; such as the Tunguskan air burst in Siberia, which leveled several square miles of forest [Near-Earth, 2003]. With the advances in telescope technology detection of large NEOs, over 1 km in size, became probable in the 90s and the possibility to overt a cataclysmic impact became a reality. The U.S. Congress took steps to protect Earth and the nation in two mandates it put forth in 1998 and 2006 [Catalina, 2008]. These two mandates require the discovery and cataloguing of 90 percent of NEOs over 140 meters in diameter [Catalina, 2008].

1.2 Research Objectives

The objective of my research is to show an improvement in the process to detect NEOs. The current detection techniques use Rayleigh sampling and a standard threshold

detector [Near-Earth, 2003]. The process described in this paper should improve the detection capability. Computer simulations using the MatLab computer language should show an increased detection rate using Nyquist sampling and a cross-correlation technique using a PSF image calculated from the atmospheric seeing parameter at the time of data collection. While an increased sampling rate will reduce the number of photons from the NEO in any pixel, it will produce a PSF that is better defined and will therefore be more spatially invariant as the NEO moves within the CCD pixel FOV. This spatial invariance allows the use of cross-correlation to depress the background noise while keeping the NEO signal intact and therefore result in a greater detection probability. This will allow for NEOs with higher visual magnitudes to be detected.

1.3 Chapter Summary

NEO detection is of national and world importance. This thesis describes a technique to improve on detection probability of NEOs greater than 140 meters in diameter using Nyquist sampling and cross-correlation with a PSF calculated from the atmospheric seeing parameter at time of data collection.

II. Literature Review

Chapter Overview

This chapter defines a NEO, describes the scientific teams involved in the detection of NEOs, how these teams were formed, and the NEO search to date.

NEOs

A NEO is defined as a comet or asteroid that comes within 1.3 AU of Earth or whose orbit brings it within 1.3 AU of Earth's orbit [Near-Earth, 2003].

NEO Scientific Definition Team

Congress mandated the National Air and Space Administration (NASA) to form a NEO Science Definition Team on August 28, 1998 [Near-Earth, 2003]. The congressional mandate called for detection of 90 percent of NEOs over 1 km in size [Evans, 2003]. Congress further mandated the discovery of 90 percent of NEOs over the size of 140 meters in June, 2006 [Catalina, 2008].

The NEO Science Definition Team has members from several leading institutions on NEO discovery including Massachusetts Institute of Technology (MIT), NASA, Department of Defense (DOD), University of Hawaii, Space Science Institute, University of Arizona, and John Hopkins University Applied Physics Lab. In their August, 22, 2003 report, they postulate that there are 1100 NEOs of size greater than 1 km and 500,000 NEOs over the size of 140 meters. NEOs greater than 1 km have an impact frequency of once every 500,000 years and NEOs over 140 meters have an impact frequency of once every 1,000 years [Near-Earth, 2003].

Their report discusses several search techniques, benefits, and costs. For ground-based telescopes, they use Lincoln Near-Earth Asteroid Research (LINEAR) as a reference for comparison for their simulation results. For a 1 meter ground-based telescope, which is the aperture diameter of the LINEAR telescope, with a one second exposure, they simulate that their limiting visual magnitude is 20.7 ± .1 for a SNR of 6 as shown in figure 1 [Near-Earth, 2003]. Figure 1 also shows LINEAR to have a limiting visual magnitude of 19.2 ± .1 [Near-Earth, 2003].

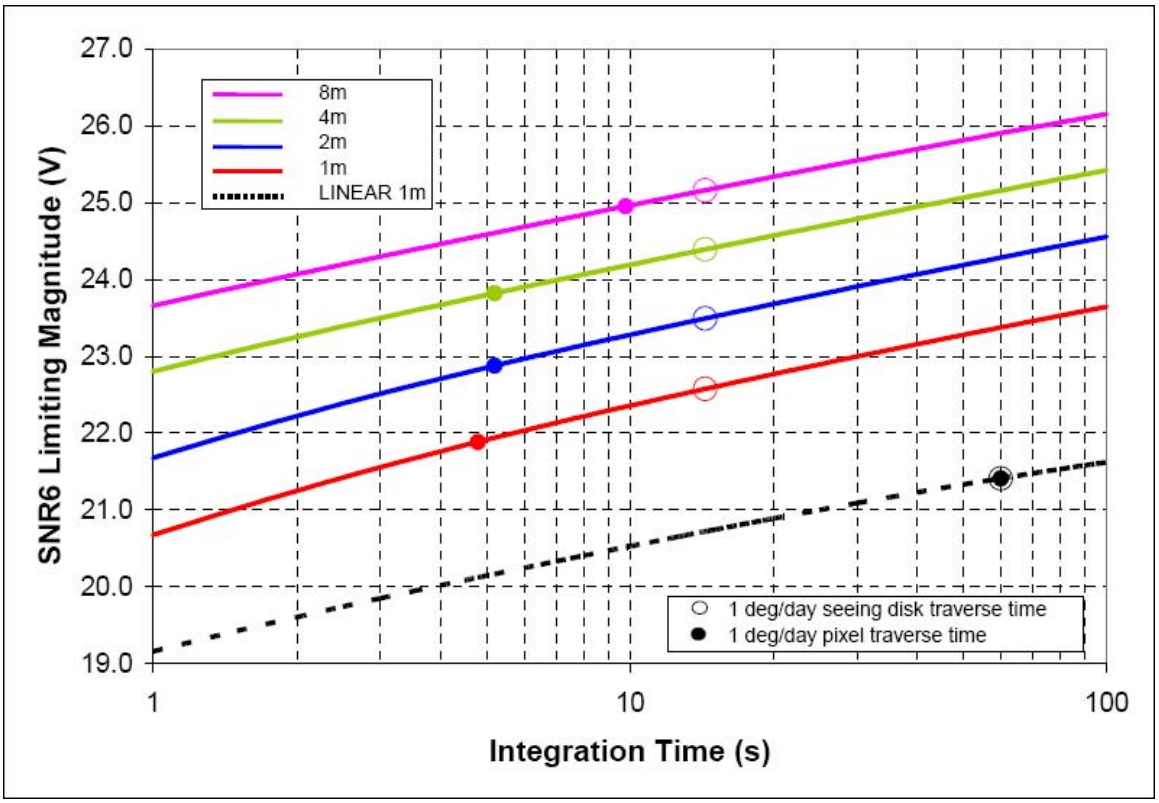

Figure 1. Limiting magnitude of ground-based sensors with 36k x 24k pixel CCD camera and LINEAR sensor for comparison [Near-Earth, 2003].

Figure 1 shows two plot points, 1 deg/day seeing disk traverse time and 1 deg/day pixel traverse time. These two points represent a NEO that moves with respect to the night sky at a rate of 1 degree per day. The 1 degree per day pixel traverse time is the amount of the time it takes the point source NEO to move through the FOV of a pixel for the CCD array used for that particular telescope aperture. The 1 degree per day seeing disk traverse time is the amount of time the PSF created by the point source NEO takes to traverse the FOV of a pixel for the CCD array used for that particular telescope aperture. It represents the time the leading edge of the PSF enters the FOV till the trailing edge exits the FOV of the pixel.

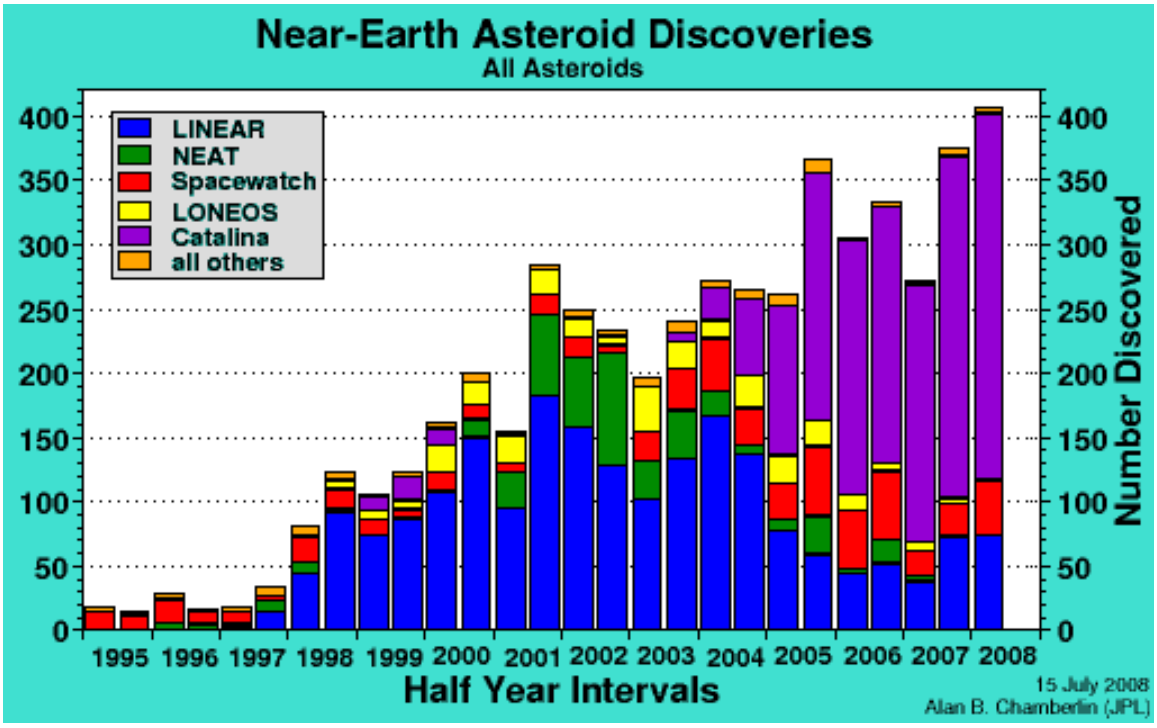

Figure 2. NEO discoveries by organization from 1995 to 2008 [NASA, 2008].

While their reports show the need for NEO detection, they do not fully fund the effort and the detection of NEOs is left to the scientific community to fulfill. The two largest endeavors, LINEAR and Catalina, are described next due to their discovery of the majority of NEOs over the past 10 years shown in the figure 2 from the NASA Jet Propulsion Laboratory (JPL) website.

Lincoln Near-Earth Asteroid Research (LINEAR)

Lincoln Laboratory at MIT formed LINEAR in association with the United States Air Force and NASA and is based in Socorro, New Mexico [Lincoln, 2008]. They currently use 2 one-meter telescopes and a .5 meter telescope for NEO detection [Lincoln, 2008]. LINEAR has been responsible for 65 percent of the NEO detections starting 1998 through the year 2003 [Evans, 2003]. While LINEAR continues to be a leading contributor to the discovery of NEOs, the NEO report of 2003 states that it may not be sufficient to detect smaller, less than 1 km in diameter, NEOs as is shown by the visual magnitude limit in figure 1 [Near-Earth, 2003].

As of December 31, 2007, LINEAR has made 22,349,515 observations in which there were 5,370,805 asteroid detections of which 225,957 where discoveries and 2,019 are categorized as NEOs [Lincoln, 2008].

Catalina Sky Survey (CSS)

The Catalina Sky Survey has three primary telescopes for use in the survey: 1.5 m on Mt. Lemmon in Arizona, 68 cm on Mt. Bigelow in Arizona, and .5 m at Siding Spring Observatory. Their mission is to fulfill the second Congressional mandate and discover 90 percent of NEOs over 140 meters in diameter [Catalina, 2008].

Since 2005, CSS has been responsible for the majority of NEO discoveries [Catalina, 2008]. I believe this is partly due to the inclusion of the telescope at Siding Spring Observatory in Australia. This is the first large telescope in the southern hemisphere to be used primarily for NEO detection.

The CSS discovered a small asteroid, 2008 TC3, less then a day from Earth impact on 6 October 2008 [Yeomans, 6 October 2008]. This is the first discovery of a NEO before Earth impact. With multiple observations from other organizations, the spin rate and trajectory were calculated. They were able to deduce the size of the asteroid to be only a few meters in diameter and therefore would burn up on impact with Earth's atmosphere and not reach the ground [Yeomans, 7 October 2008].

The asteroid entered the Earth's atmosphere on 7 October 2008 and exploded over the Northern Sudan. The resulting fireball was observed by a pilot and co-pilot of KLM [Chelsey, 2008].

This discovery and calculation is of great importance since it proves the ability of the scientific community to detect and predict NEO impacts [Yoemans, 6 October 2008].

Chapter Summary

In this chapter, we reviewed the Congressional mandates to discover 90 percent of NEOs over 140 meters in diameter, the creation of the NEO Scientific Definition Team, and the contributions of LINEAR and CSS to the discovery and cataloguing of NEOs.

III. Methodology

Chapter Overview

This chapter describes the current imaging process for detecting NEOs and the new procedure brought forth by this thesis. The current image processing technique, Rayleigh sampling with threshold detection, is discussed. The new procedure for image processing is described. In the new procedure, the Nyquist sampling image is cross-correlated with the PSF calculated from the measured seeing parameter and then processed through a threshold detector. The important topics of atmospheric seeing, point spread function, and cross-correlation are explained.

Atmospheric Seeing Parameter (r_0)

The atmospheric seeing parameter, r_0, is the parameterization of the turbulence in the atmosphere. r_0 can be measured at the time of the telescope exposure. The turbulence in the atmosphere causes photons from point sources, such as stars, asteroids, and comets, to be spatially spread out while traveling through the atmosphere. The blurring can result in photons from the point source falling into several pixels instead of just one depending on the resolution of the CCD.

The atmospheric seeing parameter, r_0, is measured in centimeters. The linear dimension in units of centimeters represents the telescope diameter that would give the limiting resolution allowed by the turbulence. Larger ground-based telescopes allow for more light collection which would result in more probable detection, but does not increase resolution. Smaller ground-based telescopes will limit the resolution.

The atmospheric seeing can be measured by pointing a laser beam into the atmosphere within the telescopes FOV and measuring the movement of it within the CCD array during data collection [Kirchner]. The atmospheric seeing parameter along with the CCD array size and visual magnitude detection limit of the telescope can be used to create a point spread function that will be used for cross-correlation.

Point Spread Function (PSF)

The PSF is the shape created by a point source whose photons travel through the atmosphere and the telescope. In astronomy, the PSF is determined by the wavelength of light being observed, the telescope configuration, and whether the telescope is ground-based or spaced-based. The image formation process can be modeled as a linear system where the input to the system is the image predicted by geometric optics (ray tracing) and the output is the 2 dimensional convolution between the input and the PSF which serves as the impulse response of the system.

For this thesis, the process is for ground-based telescopes observing optical light, .4 to .7 mm wavelength. This confines the PSF to being mostly defined by the atmosphere that the light traverses. For this reason, it is typically better to be at higher elevations to decrease the amount of atmosphere the light must travel to reach the telescope. It is also important to correctly measure the atmospheric seeing parameter to accurately calculate the PSF.

The mathematical representation of the optical transfer function (OTF) which is the two dimensional Fourier transform of the PSF for ground-based optical telescopes is given in equation (1). r_0 is the atmospheric seeing parameter, υ is the spatial frequency

variable, *f* is the focal length of the telescope forming the image onto the CCD array, and λ is the wavelength of the light being observed by the telescope [Goodman, 2000].

$$OTF(\upsilon) = e^{-3.44(\frac{\lambda f \upsilon}{r_0})^{5/3}} \quad (1)$$

Equation (1) is referred to as the long OTF since the integration time for all simulations in this thesis are much greater than .001 seconds [Goodman, 2000].

Cross-Correlation

Cross-Correlation measures the strength and direction of the linear relationship between two sets of random variables without normalizing the resulting values to between -1 and 1 [Lahti, 1998]. In these simulations, the two sets of random variables are the values contained in the matrixes of the CCD image and the calculated PSF image.

Comparison of two sets of 2-dimensional data is defined by equation (2)

$$(fg)[b,n] = \sum_{j=-\infty}^{\infty} \sum_{m=-\infty}^{\infty} f^*[j,m]g[j+b,m+n] \quad (2)$$

where one data set, f, is multiplied by another data set, g, as g is shifted with respect to f in both dimensions.

In the frequency domain, cross-correlation is defined by equation (3) where * represents the complex conjugate [Lahti, 1998].

$$cross-correlation \equiv FFT^{-1}\{FFT(A) \times FFT(B)*\} \quad (3)$$

In equation (3), A and B are signals and in this particular case the CCD and PSF images. If they are similar in form, they will cross-correlate well and produce a high value. If they are dissimilar, they will produce a lower value then if they had been similar. These values

from cross-correlation show how well the CCD image matches the PSF expected from a NEO or other point source formed by the telescope.

Rayleigh versus Nyquist

Rayleigh sampling is the empirical diffraction limit of a lens to differentiate between two point sources [Goodman, 2000]. The diffraction is caused by the light traveling through the lens which acts as a single slit. This sampling limit is given by equation (4) where D is the lens diameter in meters, lambda is the wavelength of light in meters, and theta is the angular resolution.

$$\theta = \frac{1.22\lambda}{D} \tag{4}$$

Rayleigh sampling is the limiting resolution possible by the human eye, but with computer image processing that is not necessarily the case. Rayleigh sampling is subjective and therefore not necessarily a complete description of the image [Goodman, 2000].

Nyquist sampling is defined as the largest sample period that produces a digital signal from an analog signal [Goodman, 2000]. This resolution limit is given by equation (5) where D is the lens diameter in meters, lambda is the wavelength of light in meters, and theta is the angular resolution.

$$\theta = \frac{\lambda}{2D} \tag{5}$$

Using any larger sampling will result in loss of information and aliasing [Lahti, 1998]. Using smaller sampling will not result in anymore frequency information but should more finely describe the PSF.

Current Rayleigh Detection Procedure

The process for detecting NEOs is to acquire data using Rayleigh sampling by either scanning the sky or fixed long exposure and feed the resulting CCD data into a threshold detector where the threshold is six standard deviations of the background noise [Near-Earth, 2003]. The six standard deviations of the background noise is a SNR 6.

The 2003 NEO Report gives comparisons between their theoretical calculations for detection for given telescope diameters and the limiting detection capabilities of LINEAR. Figure 1 from the 2003 NEO Report shows those comparisons. The visual magnitude limit for the NEO 1 meter telescope simulation exposure of 1 second is approximately 20.7 [Near-Earth, 2003]. The 20.7 visual magnitude value will be used as a baseline for this paper.

Figure 3 shows a representation of the PSF created by the simulation code for a 20.7 visual magnitude NEO with a seeing parameter of 14 cm taken by a 1 meter telescope with Rayleigh sampling. The NEO is centered in pixel (65, 65) and the majority of the photons, 61 percent, from the NEO are concentrated in that pixel. Some of the remaining photons reside in pixels (65, 66), (65, 64), (66, 65), and (64, 65) forming a cross shape.

The ringing emanating outward from the NEO pixel in figures 3 and 4 is caused by under sampling. Rayleigh sampling causes higher frequency components of the signal to be aliased and therefore be misrepresented as a lower frequency and results in the ringing.

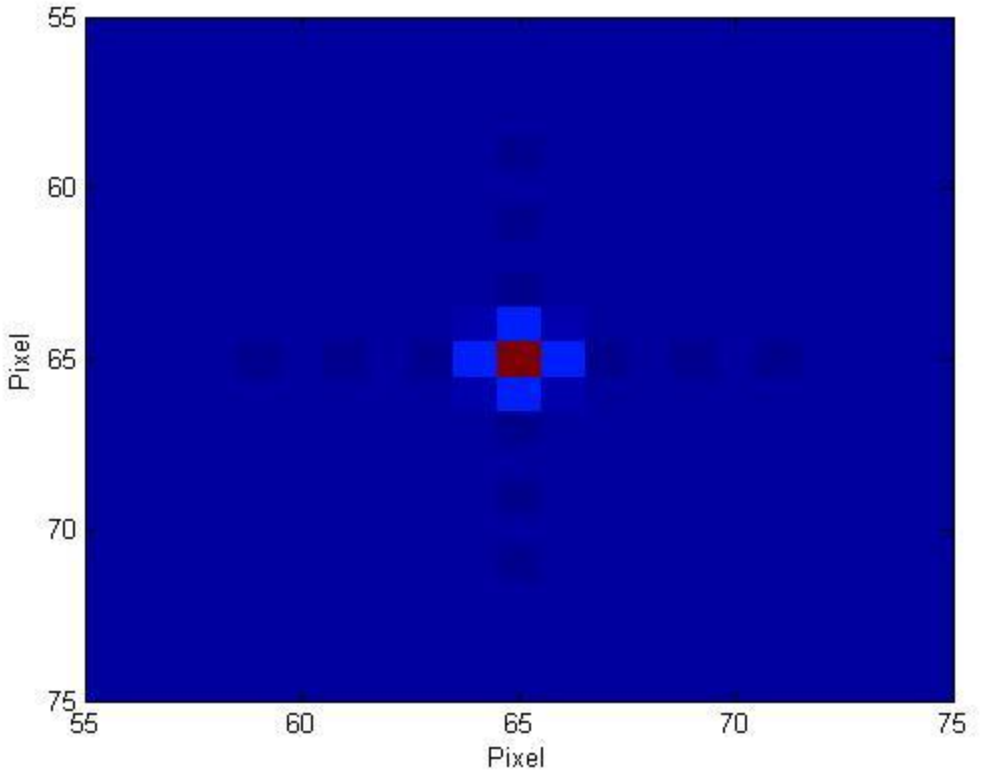

Figure 3. Image of NEO in center of pixel with Rayleigh sampling and r_0 = 14 cm.

Figures 5, 6, and 7 show the large majority of the photons that collect into pixel (65, 65) in one second of integration for Rayleigh sampling with the NEO in the center of the pixel FOV. When the NEO moves to the corner of pixel (65, 65), the photons become distributed over the four adjacent pixels: (65, 65), (65, 66), (66, 65), (66, 66) as shown in figure 4 and form the shape of a square. The maximum percentage of NEO photons in any one pixel is 30 percent. This distribution reduces the maximum number of photons into any one pixel by 55 percent for seeing of 20 cm, 51 percent for seeing of 14 cm, and 45 percent for seeing of 10 cm. These reductions should result in lower detection rates of

a NEO in the corner of a pixel for Rayleigh sampling. This drastic reduction in photons and change in the shape from a cross to a square of the PSF for Rayleigh sampling with the NEO in the corner of the pixel will not allow for cross-correlation to improve the detection rate using a PSF with a pixel centered NEO.

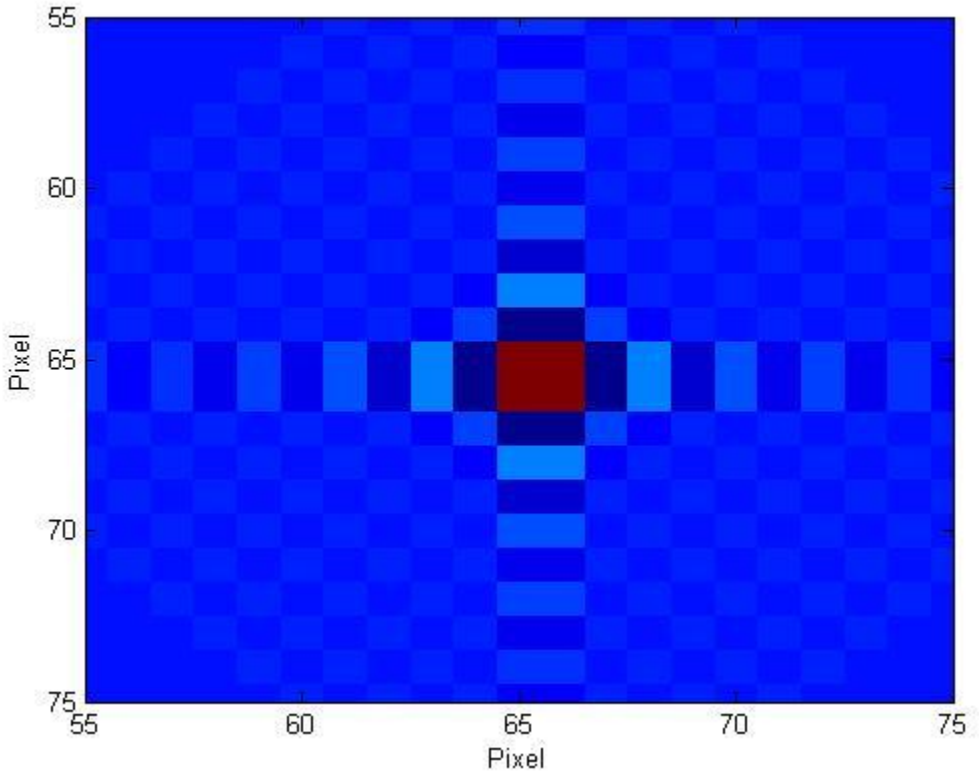

Figure 4. Image of NEO in corner of pixel with Rayleigh sampling and r_0 = 14 cm.

Nyquist with PSF Cross-Correlation Detection Procedure

The new process used in this research is to collect the CCD data using Nyquist sampling. The atmospheric turbulence is measured at the time of data collection and that

value of r_0 is used to create a PSF which is cross-correlated with the image. The resulting image will have a decreased background noise, but any NEOs or other point sources in the image will keep their intensity and therefore be more easily detected by the threshold detector.

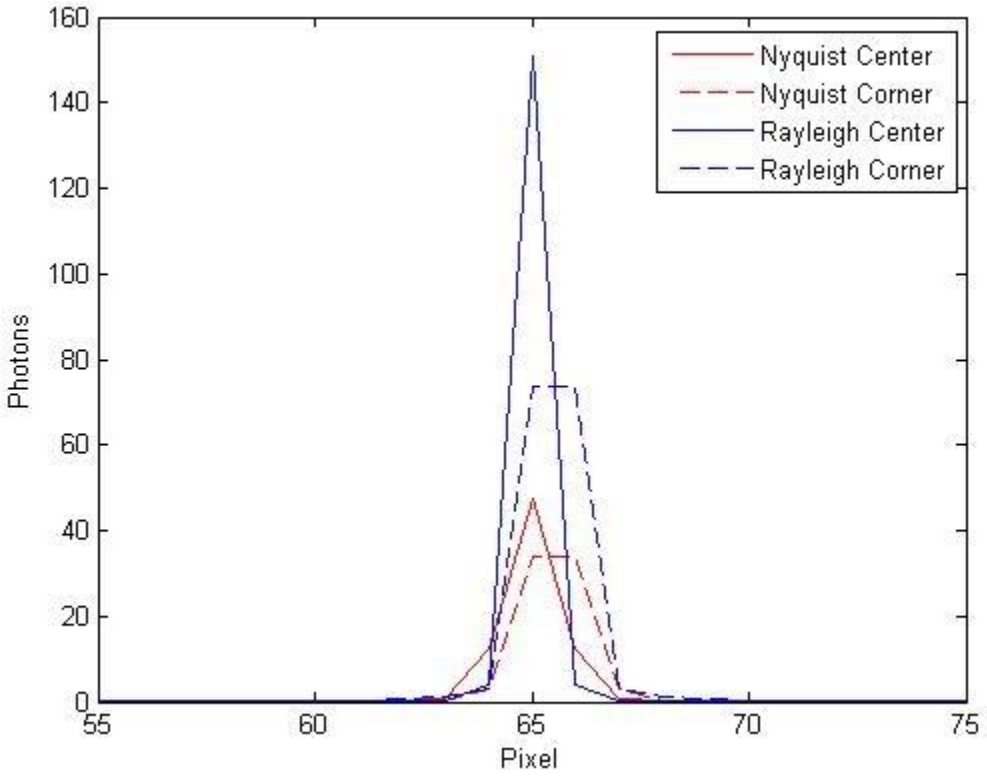

Figure 5. Photons per pixel for Rayleigh and Nyquist sampling for r_0 = 14 cm. X-axis represents the x and y coordinate of CCD array.

The telescope image will have a lower photon count per pixel due to the Nyquist sampling used for data collection than Rayleigh sampling. The percentage of NEO

photons in any one pixel for a NEO centered in pixel FOV is 19 percent and for a NEO in the corner of the pixel FOV is 14 percent for an r_0 of 14 cm. This reduction in photon count per pixel can be seen in figures 5, 6, and 7. Nyquist sampling results in greater photon per pixel percentage reduction from a seeing value of 20 cm to 10 cm than Rayleigh sampling. This distribution of photons reduces the maximum number of photons into any one pixel by 40 percent for seeing of 20 cm, 28 percent for seeing of 14 cm, and 16 percent for seeing of 10 cm.

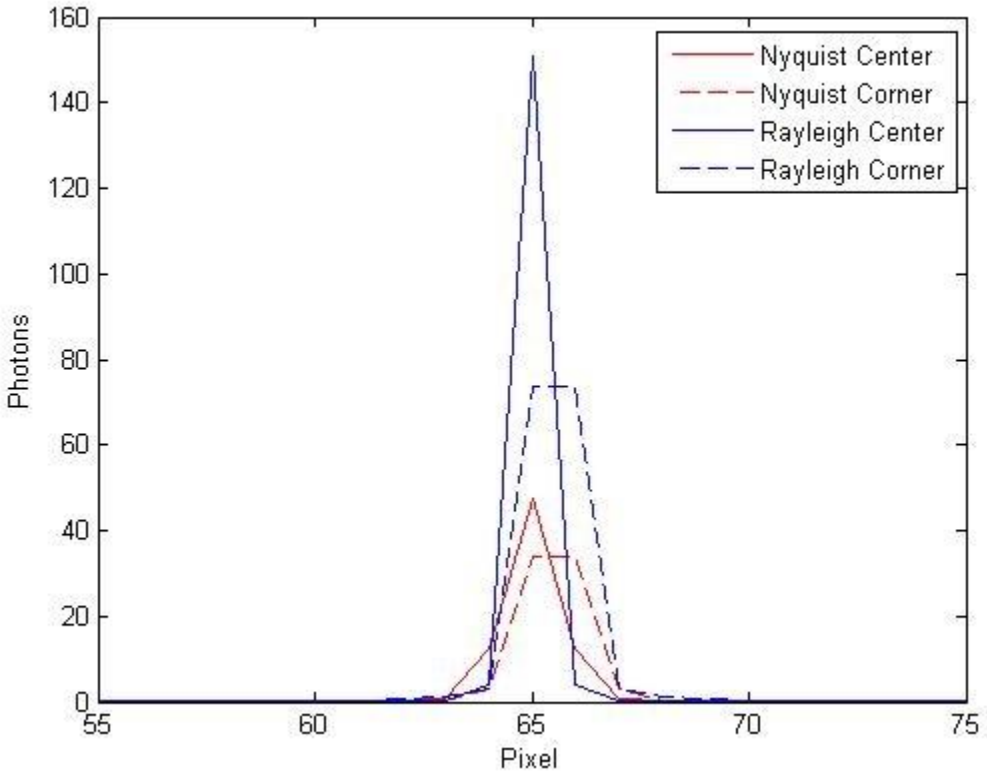

Figure 6. Photons per pixel for Rayleigh and Nyquist sampling for r_0 = 14 cm. X-axis represents the x and y coordinate of CCD array.

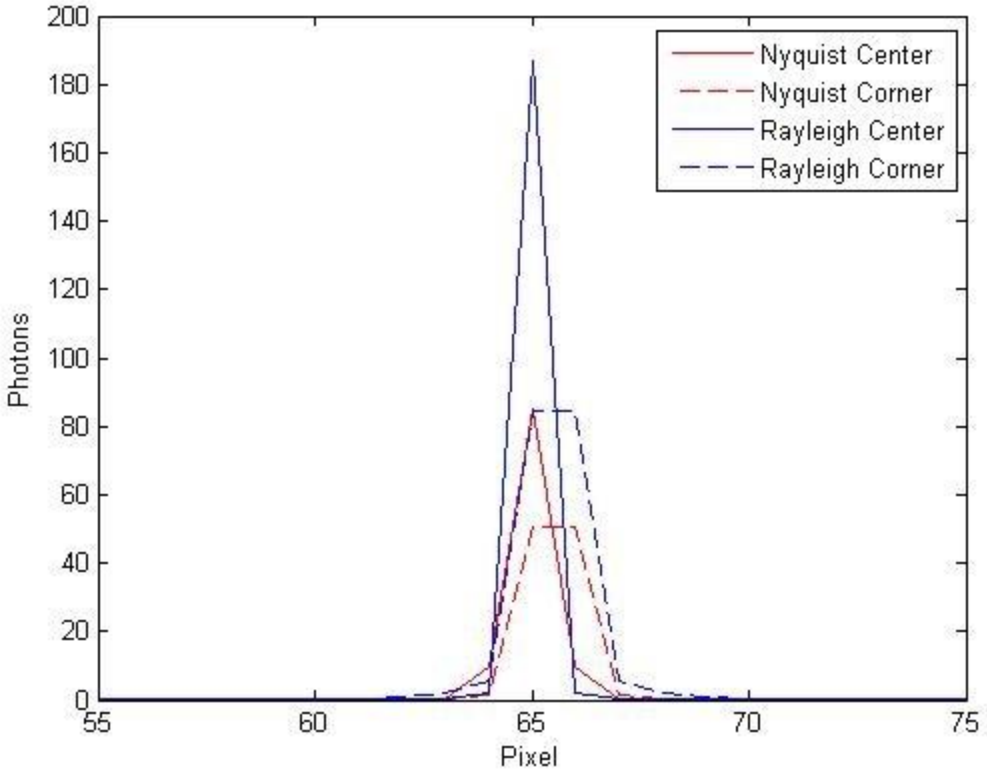

Figure 7. Photons per pixel for Rayleigh and Nyquist sampling for r_0 = 20 cm. X-axis represents the x and y coordinates of CCD array.

These deficits can be overcome by three factors. The first is Nyquist sampling also reduces the background level per pixel. The second is the greater sampling results in a more defined shape of the PSF allowing for better cross-correlation. The third is Nyquist sampling has a smaller change in photon count per pixel for the PSF from a NEO in the center of the pixel FOV to a NEO in the corner of the pixel FOV than Rayleigh sampling as seen in figures 5, 6, and 7. This smaller change allows for the PSF to retain it's shape whether the NEO is in the center or the corner of the pixel FOV as shown in

figures 8 and 9. That allows cross-correlation to perform well in either case of the NEO being in the center or corner of the pixel FOV.

The individual steps for this procedure are described for this paper's simulations. The telescope diameter, d, used for these simulations was 1 meter with an area of .785 square meters. An integration time of 1 second is standard for all data sets. 1000 background images and 1000 images with a NEO source present were generated for each data set for statistical purposes. The number of images was kept lower to allow faster computation.

A CCD rectangular grid with 128-by-128 pixels was used for all simulations. The size of the CCD array was limited due to computational limits available for these simulations. The quantum efficiency of the CCD is 66 percent to agree with NEO report simulations [Near-Earth, 2003]. Also, a detection limitation of SNR 6 is used for comparison purposes to the NEO report [Near-Earth, 2003].

The spatial cutoff frequency, f_c, is given by equation (6) where λ is the wavelength of visible light, d is the diameter of the telescope, and z_i is the focal length.

$$f_c \equiv \frac{d}{\lambda z_i} \tag{6}$$

The Nyquist sampling, f_s, given by equation (7) is defined as 2 times the cutoff frequency.

$$f_s \equiv \frac{2d}{\lambda z_i} \tag{7}$$

Atmospheric seeing can limit the resolution possible by the telescope. If the diameter of the telescope is greater than the seeing parameter, r_0, the seeing parameter replaces the diameter in the Nyquist equation as shown in equation (8).

$$f_c \equiv \frac{2r_0}{\lambda z_i} \tag{8}$$

The inverse of equation (8) is the pixel size, Δ, defined by equation (9).

$$\Delta \equiv \frac{\lambda z_i}{2r_0} \tag{9}$$

The individual pixel angle, Δ_θ, which is used for this paper's approach, is defined by equation (10).

$$\Delta_\theta \equiv \frac{\lambda}{2r_0} \tag{10}$$

The pixel angle used in the NEO report is given in equation (11).

$$\Delta_\theta \equiv \frac{1.22\lambda}{r_0} \tag{11}$$

The difference in pixel angle between the two resolutions results in more photons from the NEO being contained in fewer pixels for equation (11) than for equation (10). The pixel angle difference also means more background photons will be collected in the pixels from Rayleigh sampling than for Nyquist sampling.

To compute the number of photons reaching the telescope from the NEO, a visual magnitude approach was used for comparison purposes with the NEO report. The baseline for a zero magnitude object is Vega [Fix, 1995]. Vega's temperature, 9602 Kelvin, was used to compute the spectral luminosity of the star

$$L \equiv \frac{200hc^2\sigma^3}{e^{\frac{hc\sigma}{k_bT}} - 1} \tag{12}$$

[Fix, 1995]. Although Vega's temperature is different than our Sun, the brightness of two visual magnitude stars of the same magnitude are equal even though the amount of energy at any one wavelength may be different.

For the simulations, wavelength dependence of the visible light is not considered and CCD wavelength dependence for detection is not factored into the simulation.

In equation (12), T is the temperature of the star, h is Plank's constant, k_b is Boltzmann's constant, σ is the wave number of the light being emitted by the star, and c is the speed of light. The power for each discrete spectral bin is computed by multiplying the luminosity of each bin by the surface area of Vega [Fix, 1995].

The power is then spread over the surface area of a sphere with the radius of the distance from Earth to Vega. This is the flux that is incident on the telescope. The flux is multiplied by the area of the telescope lens, .785 square meters, to find the incident power.

The incident power of each discrete spectral bin is divided by the specific power necessary for a photon at that wavelength in equation (13).

$$energy \equiv \frac{1}{ch\sigma} \tag{13}$$

With the number of photons in each spectral bin computed, they are summed together to find the total number of photons in the visible band received from Vega. To calculate the number of photons from a NEO with a specific visual magnitude (v), the

number of photons calculated for the baseline zero magnitude Vega is divided by 2.512 to the visual magnitude power given by equation (14):

$$photons(\upsilon) = \frac{photons}{2.512^{\upsilon}} \tag{14}$$

The same equation is used to calculate the number of photons for the background with a particular visual magnitude.

The photon number from the NEO is multiplied by the integration time of the exposure. This value is used along with the seeing parameter, r_0, the pixel resolution, dx, and the CCD size to create a point spread function. The resulting PSF will be a 128-by-128 matrix which represents the CCD. The PSF for a center of pixel FOV is shown in figure 8.

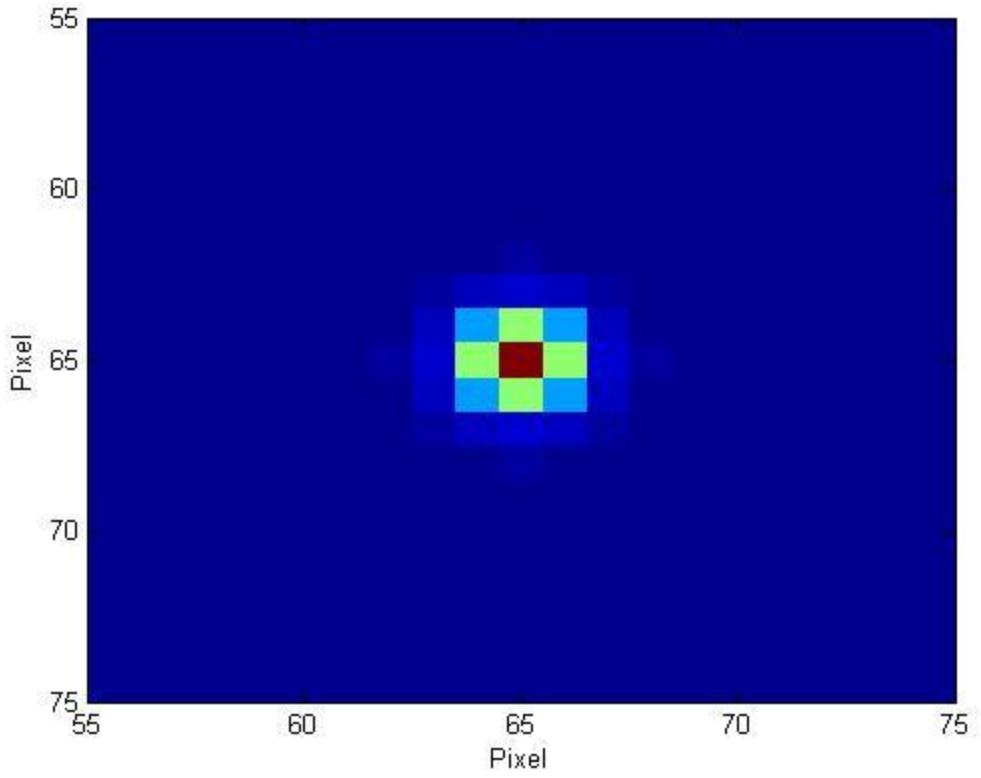

Figure 8. Image of NEO in center of pixel with Nyquist sampling and r_0 = 14 cm.

The PSF for a NEO in the corner of the pixel FOV is shown in figure 9.

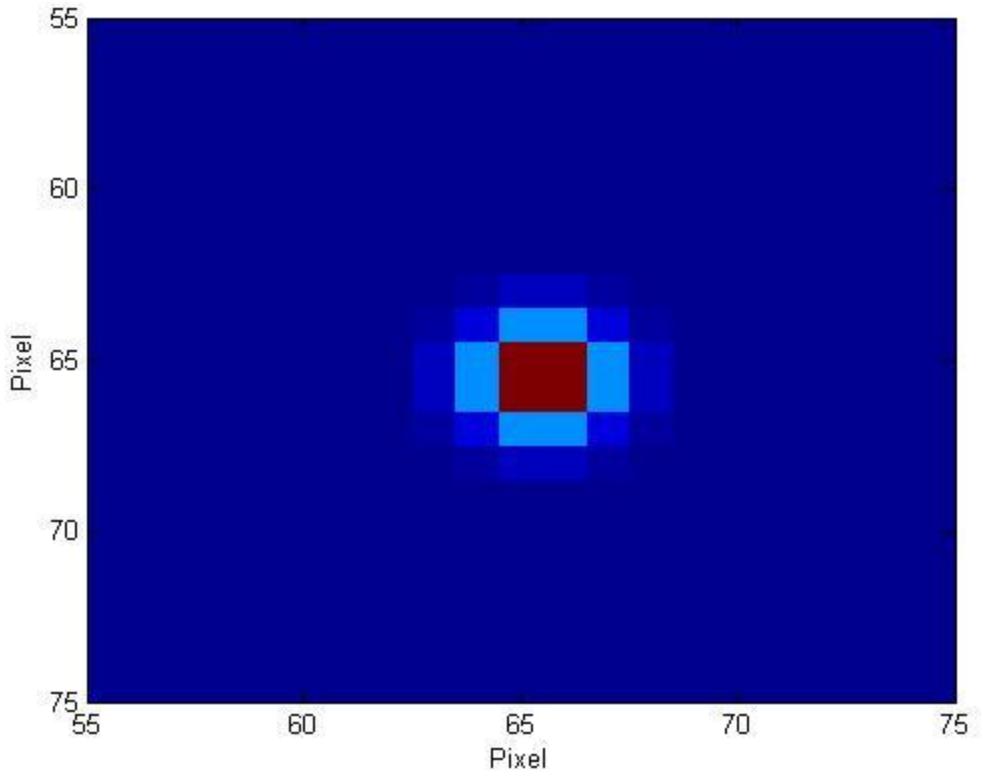

Figure 9. Image of NEO in corner of pixel with Nyquist sampling and r_0 = 14 cm.

The background is created by taking the number of photons calculated from equation (14) multiplying it by the integration time. Due to the pixel angle difference between the two approaches, the Rayleigh sampling will have a background visual magnitude of 19.5 while the Nyquist sampling will have a background visual magnitude of 21.4.

This difference in the background intensity is found by dividing equation (4) by equation (5) as shown in equation (15) and squaring the value since the CCD has two dimensions.

$$2.44 = \frac{1.22\lambda}{D} \Big/ \frac{\lambda}{2D} \tag{15}$$

Then using equation (14), the difference in visual magnitude can be found as shown in equation (16).

$$2.44^2 = 2.512^x \Rightarrow x = 2\frac{\ln(2.44)}{\ln(2.512)} = 1.94 \tag{16}$$

The image is created by adding each corresponding entry from the two matrixes together. Noise is introduced by using the *poissrnd* function in MatLab to produce a Poisson random variable noise to the data [Goodman, 2000]. An example of a CCD 128-by-128 image with a NEO in pixel (65, 65) with background Poisson noise using Nyquist sampling is shown in figure 10.

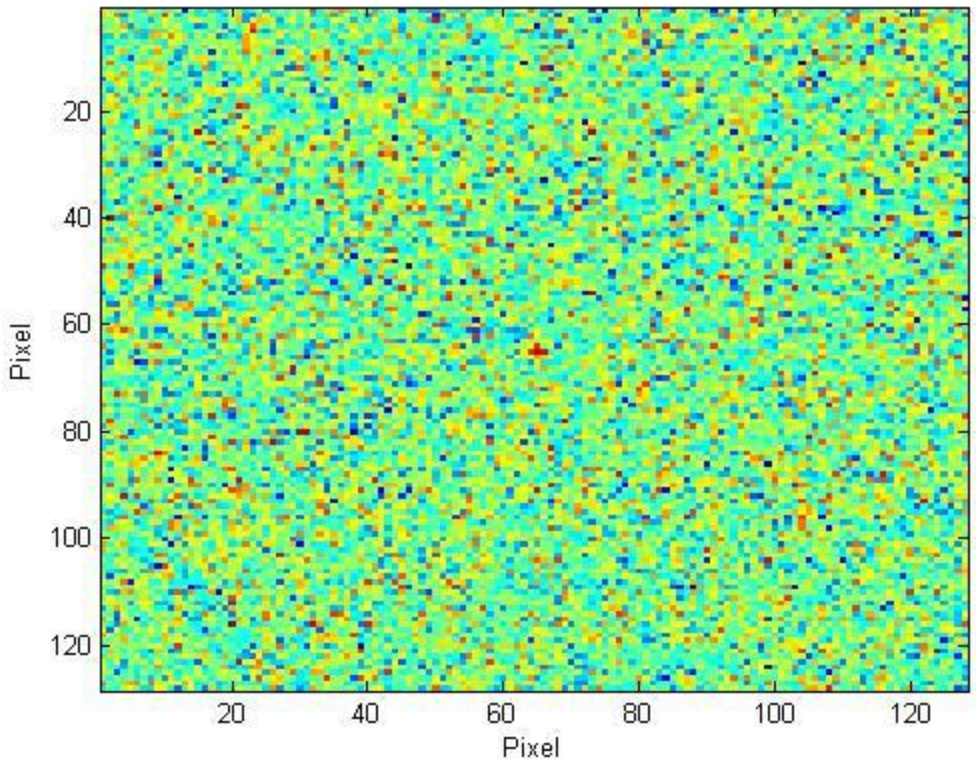

Figure 10. Image of a NEO in center of pixel (65, 65) with Nyquist sampling and r_0 = 14 cm.

The background per pixel value calculated earlier is now subtracted from the image and the background image.

To perform the cross-correlation given by equation (3), the Fast Fourier Transform (FFT) of the image, background, and PSF is performed. The FFT of the PSF is multiplied by the complex conjugate of the FFT of the image then the inverse FFT is performed and only the real part is kept. An example of the resulting image is shown in figure 11. Separately, the FFT of the PSF is also multiplied by the complex conjugate of

the FFT of the background image then the inverse FFT is performed and the real part of the result is kept.

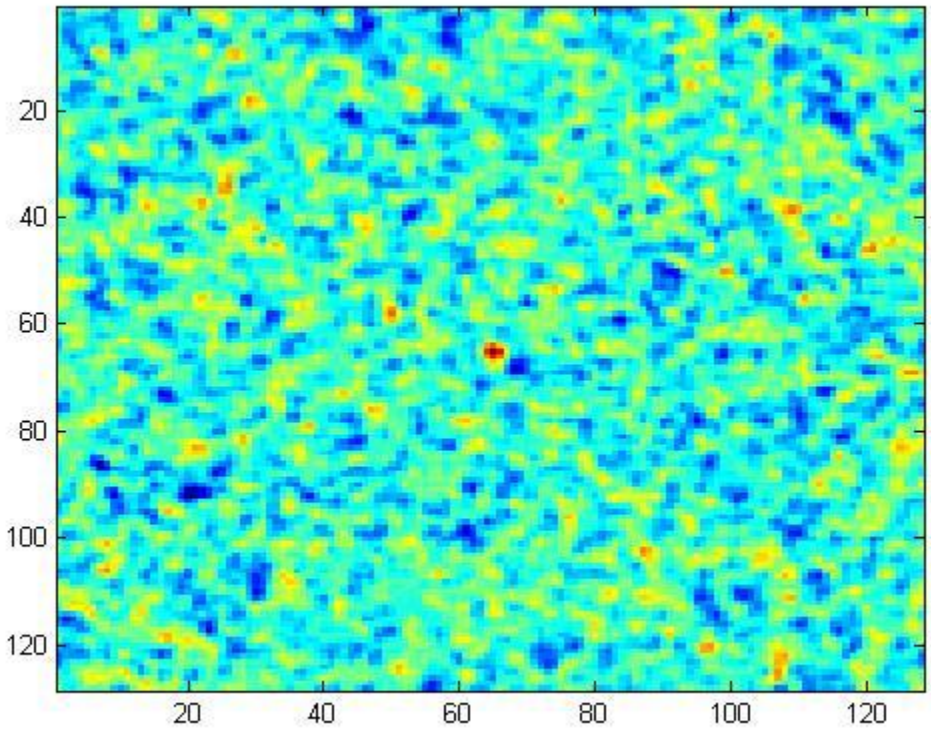

Figure 11. Image of NEO in center of pixel with Nyquist sampling and r_0 = 14 cm. after cross-correlation with PSF.

The PSF used for cross-correlation is created with the NEO source in the center of a pixel, shown in figure 8. This is regardless of the position of the NEO source used in the creation of the image.

Using these two cross-correlated matrixes, the image and background, a threshold detection technique can be used to determine if a signal is present. First, the standard deviation of the background, equation (17),

$$\sigma \equiv \frac{sqrt[\sum_1^N \sum_1^N (x_{ij} - X)^2]}{N} \tag{17}$$

must be calculated using the values from the cross-correlated background matrix, x_{ij} where i and j are the coordinates of the two dimensional matrix, the mean of that matrix, X, and the number of pixels in one dimension of the symmetrical CCD, N. Finally the average of the standard deviations is computed by summing the standard deviation values from each background image and dividing that value by the total number of background images. This value is referred to as the signal-to-noise ratio (SNR). With this, the value of the SNR 6 can be computed by multiplying the standard deviation of the correlated background matrix by 6. This value is the threshold for the threshold detector.

The threshold detector works by comparing each value in both the correlated image and background to the threshold value. Any value above the threshold value is considered a detection. This is considered a positive recognition of a source, the NEO. If the detection is in the background, it is a false alarm and is cataloged as such. If the detection occurs in the image, it is a positive alarm and is cataloged as such.

The false alarm rate, P_f, for a Gaussian distribution is

$$P_f = 1 - \frac{1}{\sigma\sqrt{2\pi}} \int_{-\infty}^{a} e^{-\frac{(u-\mu)^2}{2\sigma^2}} \, du \tag{18}$$

where a is the SNR value. At SNR 6, a equals 6, for example. Where μ, the mean, is equal to 0 and σ=1/2, equation (18) becomes

$$P_f = 1 - \frac{2}{\sqrt{2\pi}} \int_{-\infty}^{a} e^{-2u^2} du \,. \quad (19)$$

Only positive values are possible for the false alarm rate so the integration can begin at zero instead of negative infinity. This excludes half of the Gaussian distribution and substituting $t=u/2^{1/2}$ equation (19) becomes

$$P_f = .5 - \frac{2}{2\sqrt{\pi}} \int_{0}^{\frac{a}{\sqrt{2}}} e^{-t^2} dt \,. \quad (20)$$

At SNR 6, the theoretical Gaussian false alarm rate, P_f, for each pixel of the matrix is 9.866x10^-10, calculated by equation (20). Gaussian calculations can be used as an approximation for Poisson given the same mean and variance [Young, 1962]. The total number of pixels for 1000 images of 128-by-128 CCDs is 1.6384×10^7. The theoretical false alarm value is important for a validity check versus the simulated values of false alarm rate per pixel. The number of pixels only allows for a minimum false alarm rate of 6.1035×10^{-8} without going to zero.

An acceptable detection rate is considered to be 90% and above as is stated in the NEO report [Near-Earth, 2003].

Chapter Summary

This chapter defined important concepts and described the procedure for photons reflected by a NEO to reach the telescope CCD. The CCD image is then cross-correlated with a PSF calculated from the atmospheric seeing parameter. The pixels from the cross-correlated image are then tested versus a threshold value based on the SNR of the cross-correlated background.

IV. Results and Discussion

Chapter Overview

This chapter presents the results of the thesis. The probability of detection of a NEO for the process described in Chapter 3 is given for the NEO in the center of a pixel, centered-edge of a pixel, and corner of a pixel for both Nyquist sampling with cross-correlation of a PSF and Rayleigh sampling. Nyquist sampling with cross-correlation of a PSF is shown to be an improvement over Rayleigh sampling for all cases.

Data Analysis

Data sets were simulated for a point source NEO in the center of the FOV of a pixel, centered-edge of a pixel, corner of pixel, and several other situations. Atmospheric seeing values of 14 cm were used in the simulations unless specified. Most data sets were run for both Nyquist sampling with PSF cross-correlation and Rayleigh sampling for comparison. 1000 images with the NEO present and 1000 background only images were created and used for each simulation. Typically, each simulation calculates the probability of detection and false alarm rate per pixel for SNR 3 to 6 by increments of .05. SNR represents the number of standard deviations of the background that is used as a threshold for detection.

The computation time necessary for each simulation was 20 minutes ± 5 minutes for one ACER laptop with a 1.6 GHz processor with 2 Gigabytes or RAM with a dual bus. Due to the simulation time and the number of different data inputs incorporated into this thesis, multiple simulations for the same data inputs were not incorporated into this thesis. The large sample size, 1000 images, was used for statistical purposes.

The MatLab code is included in Appendix 1 for reference; the specifics of each simulation may require changes in the code.

Rayleigh Sampling with and without Cross-Correlation

Figure 12 shows the result of using cross-correlation with a PSF for Rayleigh sampling for a NEO in the corner of the pixel FOV. The PSF used for cross-correlation was for a NEO centered in the pixel FOV. The cross shape PSF described by figure 3 does not cross-correlate well with the square shape NEO image from figure 4. This is evident in figure 12 by the lower probability of detection on average for the Rayleigh sampling with cross-correlation of a PSF than the Rayleigh sampling without cross-correlation. For this reason cross-correlation is not applicable to Rayleigh sampling.

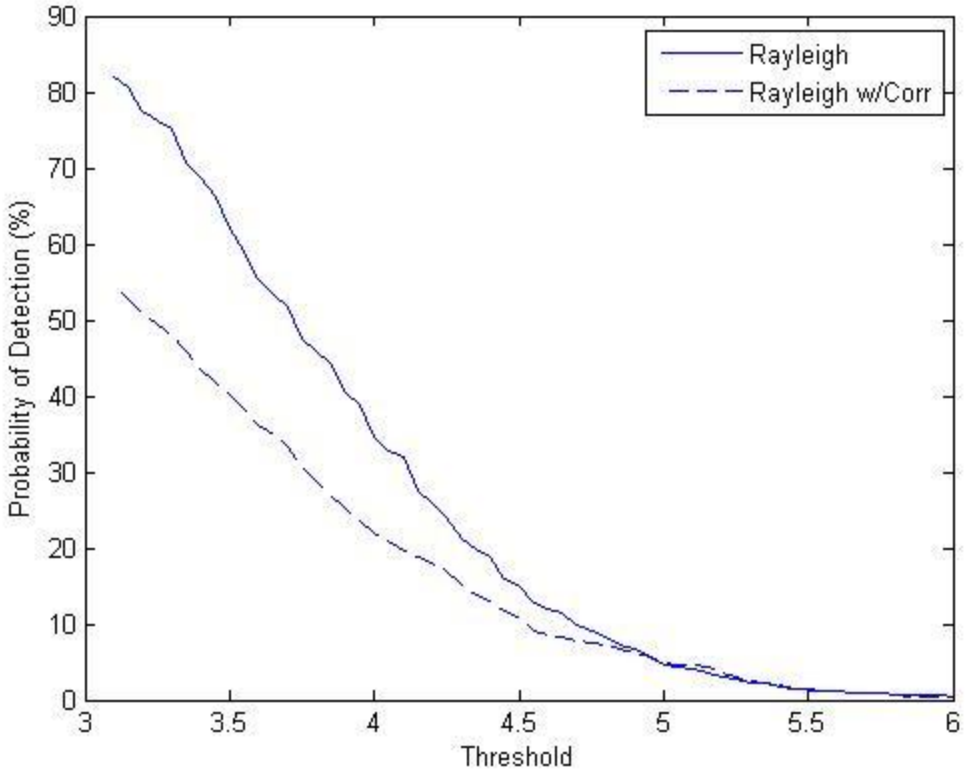

Figure 12. Rayleigh sampling with and without cross-correlation for a NEO in corner of pixel for r_0 = 14 cm.

Probability of Detection as a Function of Position in FOV of Pixel

NEO in Center of Pixel

Figure 13 shows two simulations for a NEO in the center of the pixel. The Nyquist sampling with cross-correlation of a PSF process is better than the Rayleigh sampling for all threshold values. The point where Rayleigh sampling reaches 90 percent detection rate is a threshold of 4.25. Nyquist sampling with cross-correlation reaches 90

percent detection rate at a threshold of 5.15. At a threshold of 6, Nyquist detection is 2.29 times greater than Rayleigh detection.

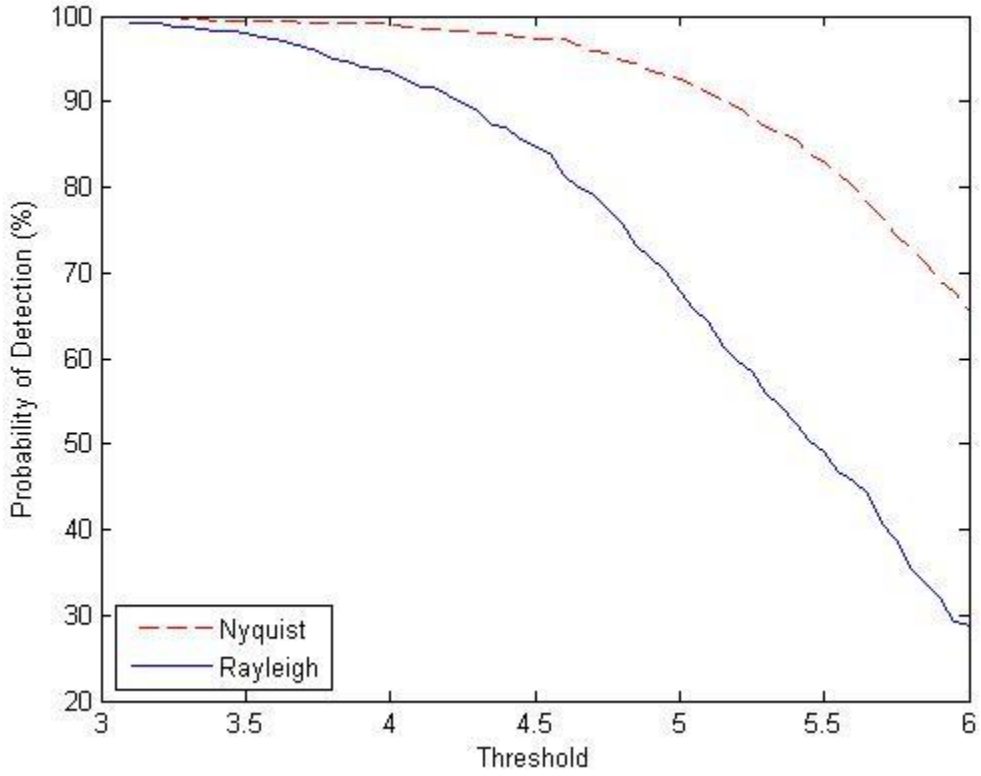

Figure 13. Probability of detection versus threshold for NEO in center of pixel with r_0 = 14 cm.

The NEO source in the center of the pixel is the best case scenario for detection probability for both Nyquist sampling with cross-correlation of a PSF and Rayleigh sampling since the maximum number of photons in any one pixel is achieved in this scenario. The cross-correlation process is most beneficial at limiting thresholds and visual

magnitudes and will allow for detection of more NEOs and specifically smaller diameter NEOs.

From figure 14, the false alarm rate for Nyquist detection is lower than Rayleigh for all detection rates.

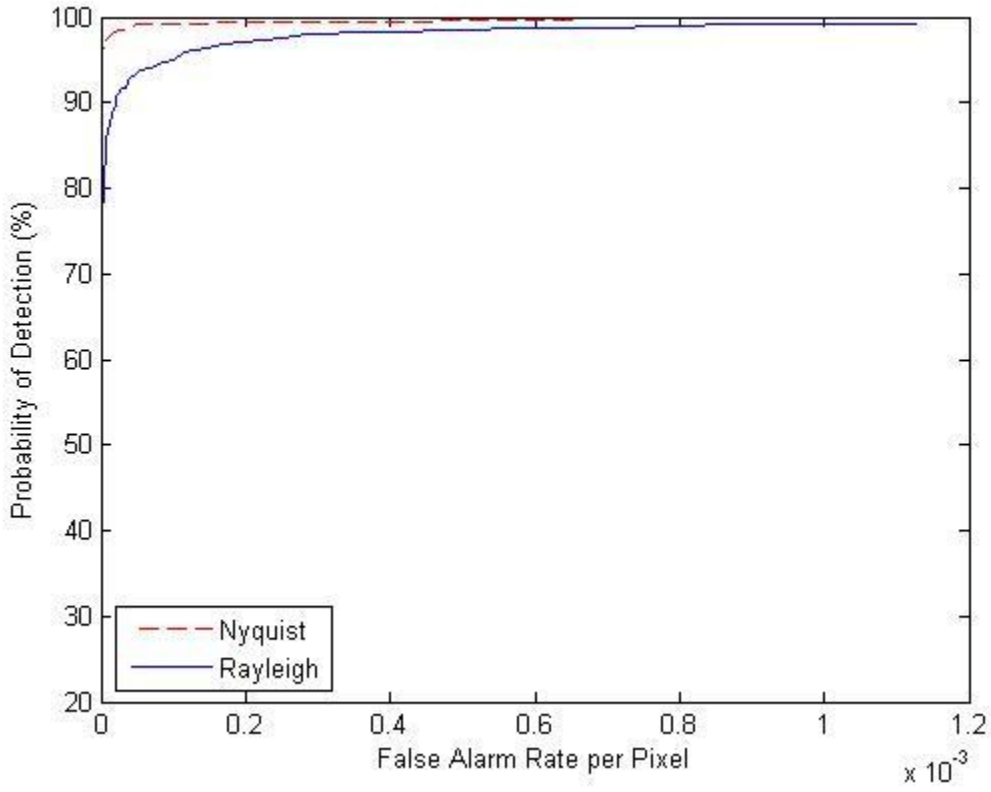

Figure 14. Probability of detection versus false alarm rate for NEO in center of pixel with r_0 = 14 cm.

NEO on Edge of Pixel

In figure 15, The Nyquist sampling with cross-correlation process is better than the Rayleigh sampling for all thresholds. The point where Rayleigh sampling reaches 90 percent detection rate is a threshold of 3.40. Nyquist sampling with cross-correlation reaches 90 percent detection rate at a threshold of 4.70. At a threshold of 6, the Nyquist detection rate is 18.6 times better than the Rayleigh. This improvement is greater than for a NEO source in the center of a pixel in figure 13. This is expected by theory due to the cross-correlation process with the PSF.

The cross-correlation with a PSF retains the intensity of the NEO but reduces the background intensity and therefore the value of the threshold of 6. This is evident in the high detection rate for Nyquist sampling with cross-correlation versus the detection rate of Rayleigh sampling alone. This benefit is reduced as the threshold value is reduced to 3 as seen in figure 15.

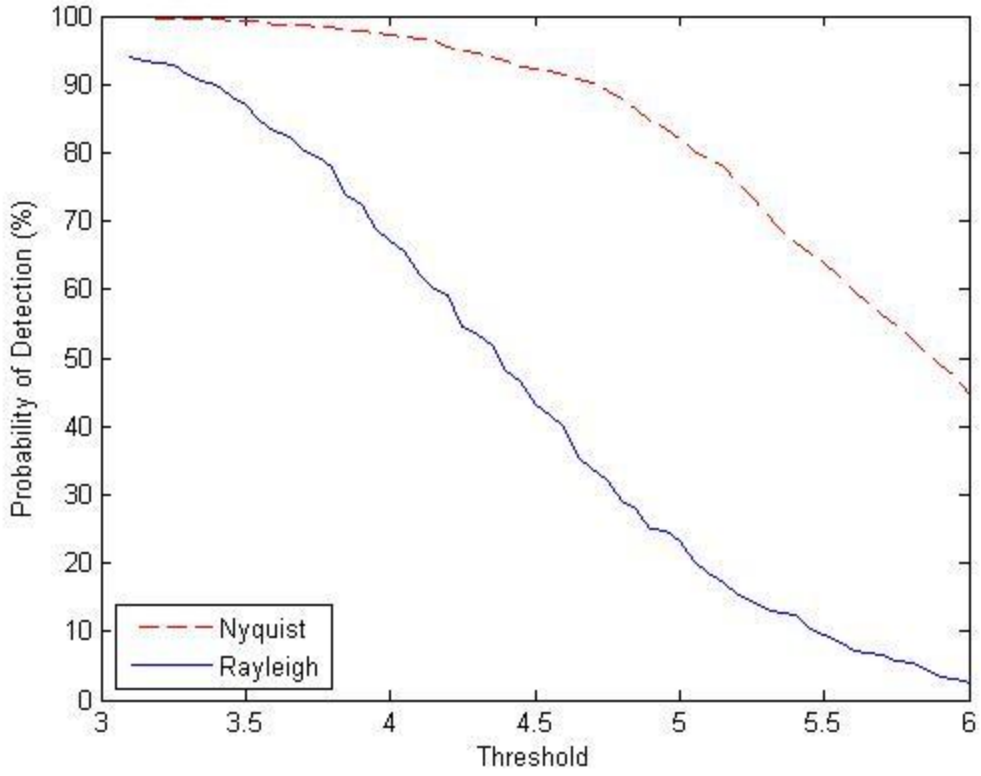

Figure 15. Probability of detection versus threshold for NEO on edge of pixel with r_0 = 14 cm.

Figure 16 shows that Nyquist sampling with cross-correlation of a PSF crosses the 90 percent detection rate probability with a false alarm rate of 1.83×10^{-6} per pixel while Rayleigh sampling reaches a false alarm rate of 4.08×10^{-4} per pixel for a detection probability rate of 90 percent.

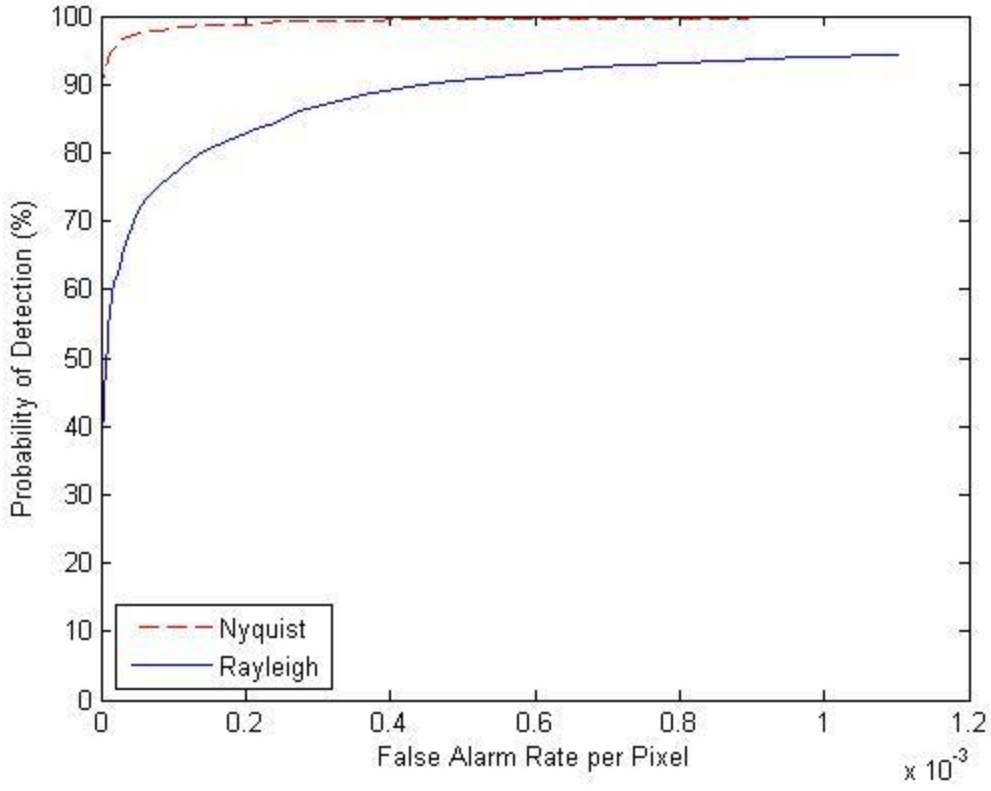

Figure 16. Probability of Detection versus Probability of False Alarm for NEO on edge of pixel with r_0 = 14 cm.

From figure 16, the lower false alarm rate for Nyquist sampling with cross-correlation of a PSF shows the importance of cross-correlation in the reduction of the background noise while keeping the NEO signal nearly intact. Rayleigh sampling requires a much lower threshold in order the reach the same detection probability as Nyquist sampling with cross-correlation of a PSF. Rayleigh sampling is not able to decrease the background noise while the NEO photons are spread out over more pixels therefore reducing its intensity in any one pixel.

NEO in Corner of Pixel

The Nyquist sampling with cross-correlation process is better than the Rayleigh sampling for all threshold values in figure 17. Rayleigh sampling never reaches 90 percent detection rate. Nyquist sampling with cross-correlation reaches 90 percent detection rate at a threshold of 4.15. Rayleigh sampling detection probability reduces to zero at a threshold of 6 while Nyquist sampling with cross-correlation has a detection probability of 28 percent.

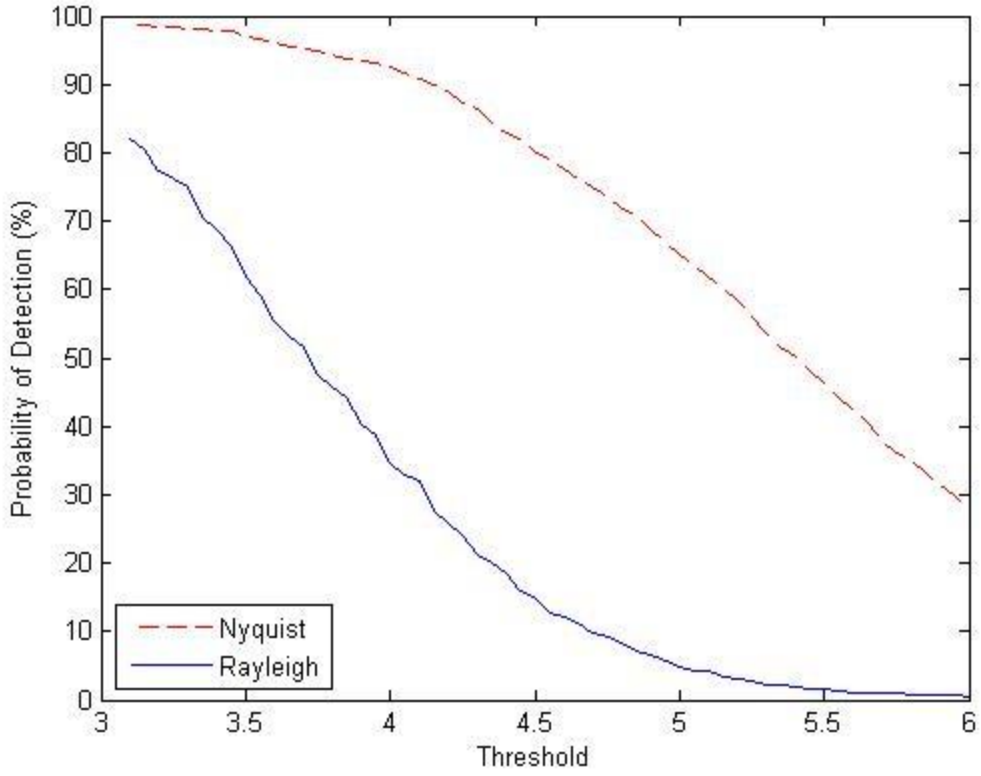

Figure 17. Probability of detection versus threshold for NEO in corner of pixel with r_0 = 14 cm.

The results from figure 17 show the greatest improvement for Nyquist sampling with cross-correlation over Rayleigh sampling. The NEO source in the corner of the pixel is the worst case scenario for detection purposes, but may be more typical for observation since the space between pixels and the edges of pixels cover more area than center of the pixel scenarios.

Figure 18 shows Nyquist sampling with PSF cross-correlation with a lower false alarm rate than Rayleigh sampling for all detection probabilities. This is evidence of the ability of cross-correlation to reduce the background and retain the NEO source signal.

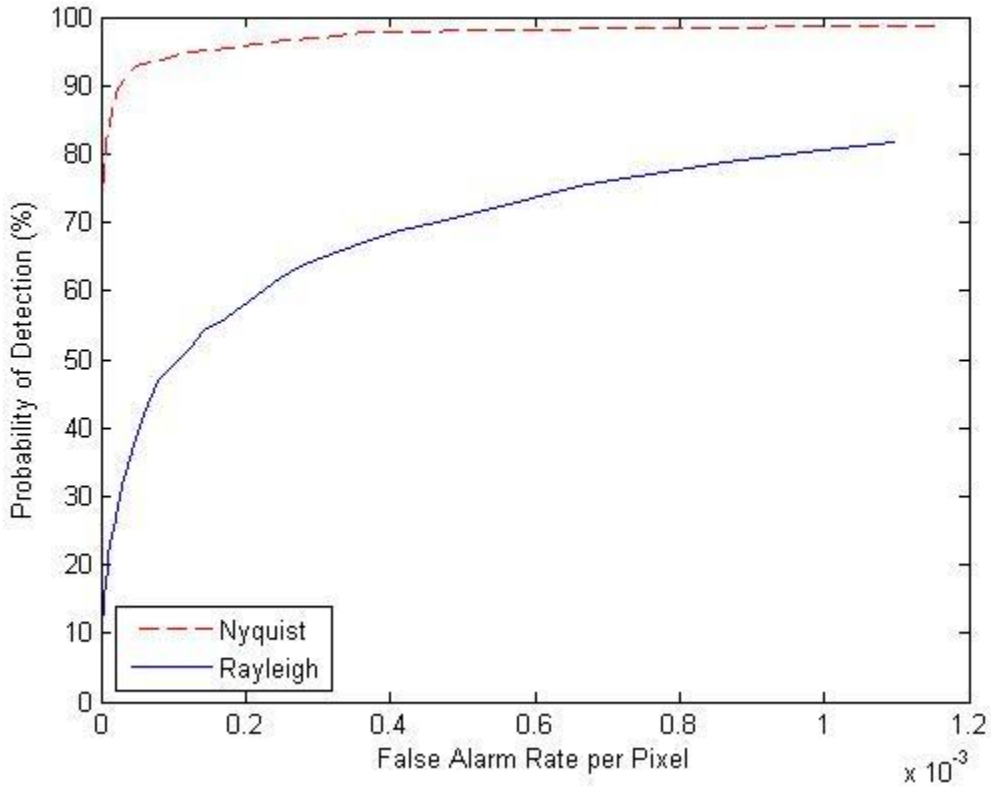

Figure 18. Probability of detection versus false alarm rate for NEO in corner of pixel with r_0 = 14 cm.

Probability of Detection as a Function of Position in Pixel

Figure 19 shows the trend in detection probability for both detection processes as a function of position in the FOV of the pixel. A threshold of 5 was used since the

Rayleigh sampling probability of detection is almost zero before the NEO reaches the corner for a threshold of 6. A threshold of 5 allows for the divergence of the two lines to be more evident as the NEO moves closer to the corner of the pixel. As the NEO moves to the corner of the CCD pixel the detection probability of the Nyquist sampling with cross-correlation of a PSF has a nearly 30 percent drop while the Rayleigh sampling drops to almost zero. This rapid decline by Rayleigh sampling and the minimal decline of Nyquist sampling with cross-correlation of a PSF are evidence of the ability of cross-correlation to retain the NEO intensity while reducing the background in order to make NEO more detectable over Rayleigh sampling with threshold detection alone.

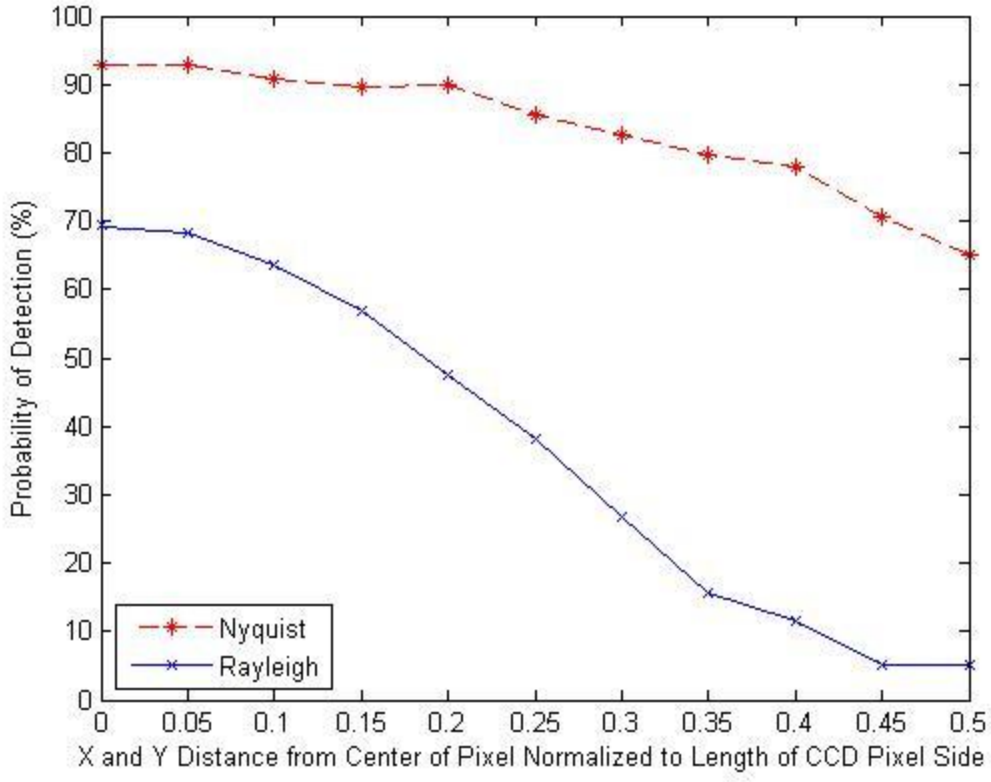

Figure 19. Probability of detection versus position in FOV of pixel. X-axis normalized to length of each side of CCD. r_0 = 14 cm and PSF of 14 cm for a threshold of 5.

Probability of Detection with Varying Seeing Parameter

Figure 20 shows two simulations for Nyquist with cross-correlation with a PSF of 14 cm. The detection threshold is set at 6 and the NEO source is located in the center and corner of pixel (65, 65) for the two separate simulations. The atmospheric seeing parameter is varied from 10 to 20 cm while the PSF used for cross-correlation is kept at a value of 14 cm.

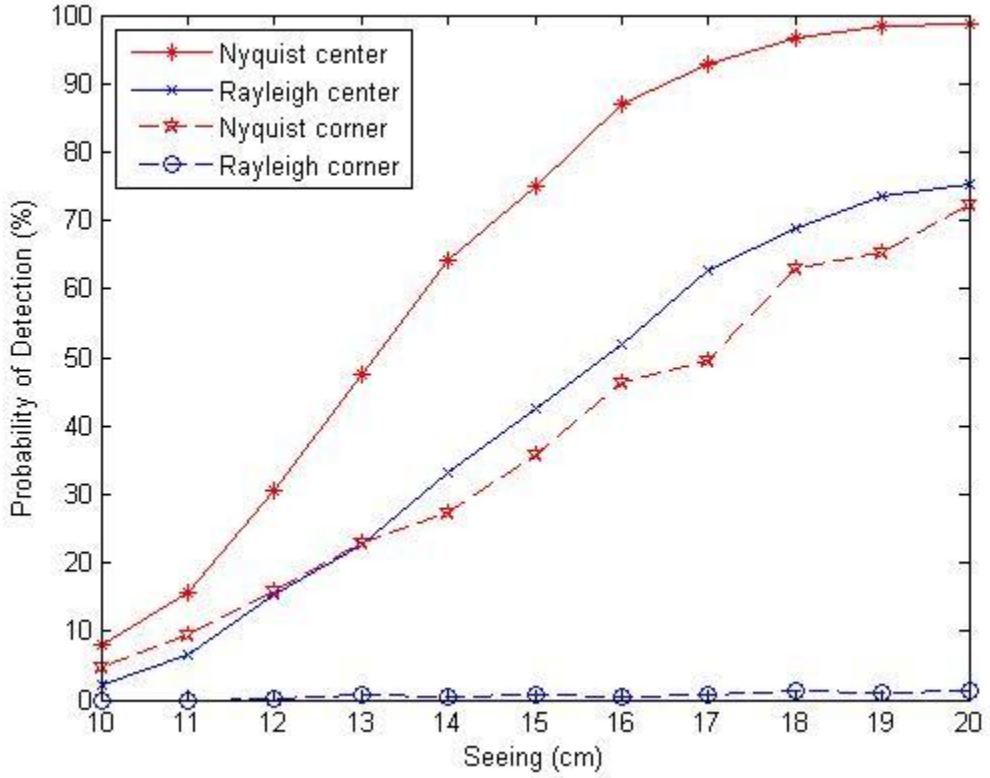

Figure 20. Probability of detection versus seeing for NEO in corner and center of pixel with PSF = 14 cm and SNR = 6.

There is no dramatic change in the detection probability curve before or after seeing of 14 cm which infers that there is no significant loss of detection probability by incorrectly calculating the atmospheric seeing parameter for calculating the PSF. The data suggests that cross-correlation with a PSF in general is most important.

Nyquist with Cross-Correlation Best Match to Rayleigh Limit

Figure 21 shows several Nyquist with cross-correlation of PSF simulations for a NEO source in the center of the pixel with a visual magnitudes varying from 20.7 to 21.0 by increments of .1. They are for comparison purposes against a Rayleigh sampling simulation with a NEO source in the center of the pixel with a visual magnitude of 20.7. The Nyquist simulation with the closest match to the detection probability of the Rayleigh simulation is the simulation with a NEO source visual magnitude of 20.9 that is an improvement of .2 magnitude or 20.5 percent.

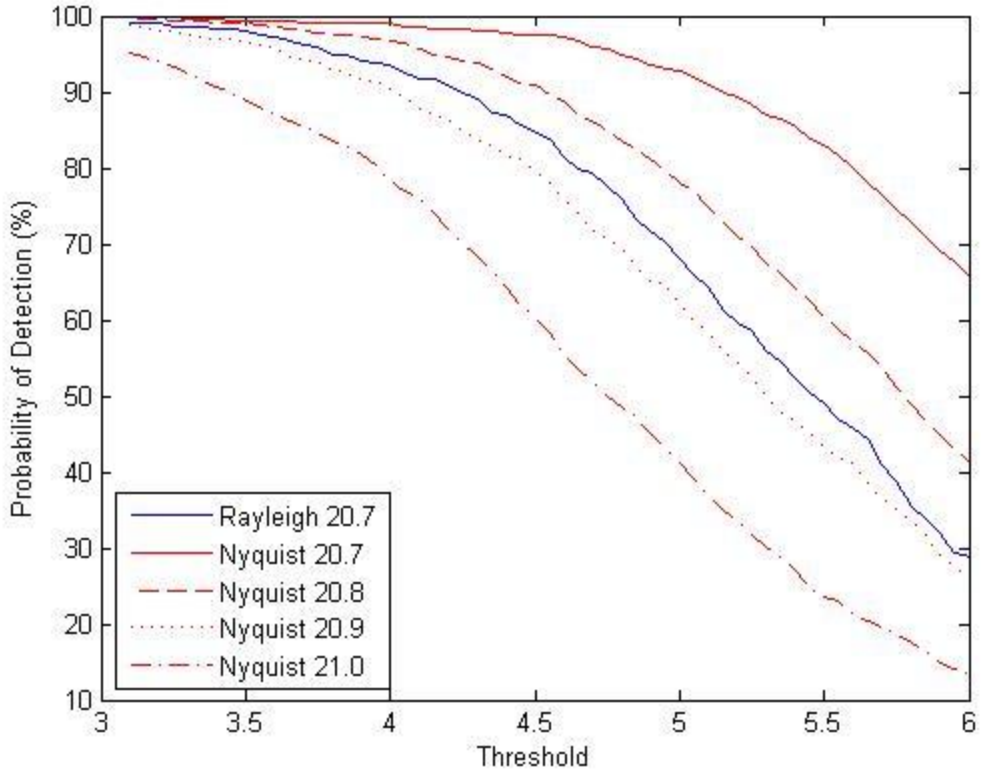

Figure 21. Best match visual magnitude limit for Nyquist with cross-correlation to Rayleigh of visual magnitude 20.7 with a NEO in center of pixel with PSF = 14 cm.

The best match was determined using the difference between the corresponding SNR detection probabilities of the Nyquist sampling with cross-correlation of a PSF and the Rayleigh sampling, taking their absolute values and summing them which is described by equation (21) where Nyquist values are X_N and Rayleigh values are X_R.

$$\sum \left| X_N - X_R \right| \tag{21}$$

The resulting values from equation (21) are 9.930 for visual magnitude 20.7, 3.964 for visual magnitude 20.8, 2.316 for visual magnitude 20.9, and 10.988 for visual magnitude 21.0.

Figure 22 shows simulations for an NEO in the corner of the pixel with an atmospheric seeing parameter of 14 cm. Several simulations of Nyquist sampling with cross-correlation of a PSF with varying NEO visual magnitudes were produced in order to find the best match to the Rayleigh sampling for a NEO visual magnitude of 20.7. No Nyquist simulation matched the false alarm rate of Rayleigh, but the Nyquist simulation of a NEO with a visual magnitude of 21.1 is the best match for the Rayleigh simulation with a NEO visual magnitude of 20.7 using equation (21). This would be an improvement of .4 visual magnitude which results in a 45.19 percent improvement in photon intensity.

From equation (21), the Nyquist sampling of a NEO visual magnitude of 21.2 with cross-correlation of a PSF is the best match for the Rayleigh sampling of a 20.7 visual magnitude NEO in figure 22. The resulting values from equation (20) are 6.368 for visual magnitude 21.0, 2.663 for visual magnitude 21.1, 3.356 for visual magnitude 21.2, and 7.021 for visual magnitude 21.3.

When only the threshold values of 4.5 to 6 are considered, the resulting values from equation (21) are 2.776 for visual magnitude 21.0, 1.323 for visual magnitude 21.1, .222 for visual magnitude 21.2, and .526 for visual magnitude 21.3. The Nyquist simulation of a NEO with a visual magnitude of 21.2 is the best match for the Rayleigh simulation with a NEO visual magnitude of 20.7 using equation (21) for threshold values of 4.5 to 6. This would be an improvement of .5 visual magnitude which results in a 59.37 percent improvement in photon intensity.

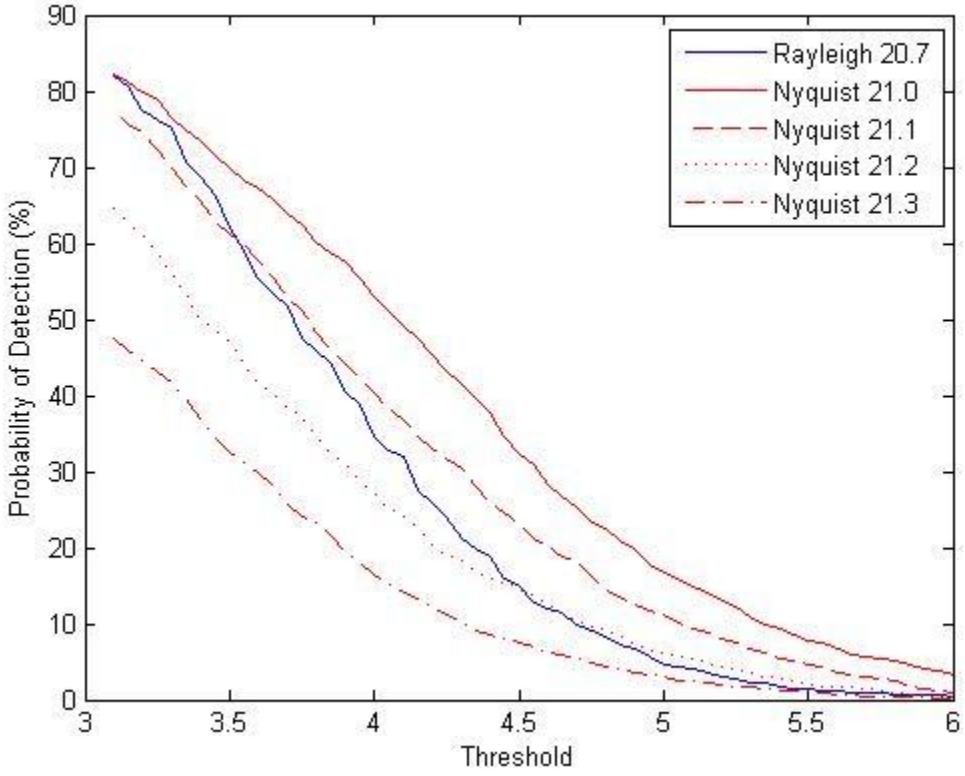

Figure 22. Best match visual magnitude limit for Nyquist with cross-correlation to Rayleigh of visual magnitude 20.7 with a NEO in corner of pixel (65, 65) with PSF = 14 cm.

False Alarm Rates

From equation (20), the false alarm rate of a threshold of 6 is 9.866×10^{-10} per pixel. Figure 23 provides a plot of the false alarm rates for Nyquist and Rayleigh sampling for center, edge, and corner of the pixel FOV. These false alarm rates are practically indistinguishable from each other.

The plot of the theoretical false alarm rate computed using equation (20) is shown for comparison and is consistently 20 percent lower than the six simulation plots. This error is acceptable since the Gaussian calculation of false alarm is an approximation of the Poisson false alarm [Young, 1962].

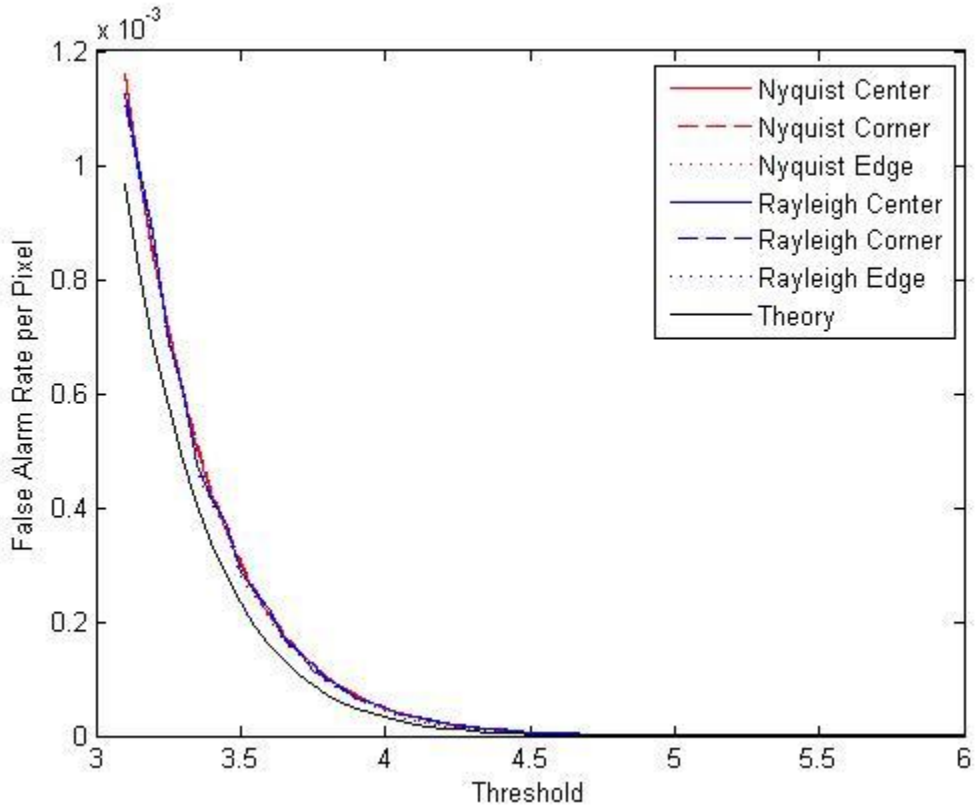

Figure 23. False alarm rates for Nyquist and Rayleigh samplings.

With ~10^7 pixels of either image or background per simulation, the false alarm rate does not register one single false on average until a threshold of 5.5. This low false alarm rate allows for a lower threshold for detection purposes then the threshold of 6

being used in the NEO report. A lower threshold would allow for higher visual magnitude NEOs to possibly be detected and increase the detection probability of those NEOs at the current visual magnitude limit of the telescope apparatus.

Figure 23 shows that there is no significant effect to the false alarm rate due to using Nyquist sampling or cross-correlation with the PSF verses Rayleigh sampling.

Chapter Summary

The Nyquist sampling with PSF cross-correlation process out-performs the Rayleigh sampling in all simulations for probability of detection. The process is most beneficial when the NEO source is near the corner of the CCD pixel with an improvement of 45.19 percent over Rayleigh sampling alone to a visual magnitude of 21.2. The process does provide a 20.5 percent improvement to a visual magnitude of 20.9 over Rayleigh sampling if the NEO is located in the center of the pixel. The false alarm rate agrees with the theoretical false alarm rate in all simulations.

V. Conclusions

Explanation of the Problem

NEOs are a threat to Earth and human existence. Their impact rates vary greatly depending on their size as does their resulting effects from 1 every 500,000 years for NEOs over 1 km in diameter to 1 every 1,000 years for NEOs over 140 m in diameter [Near-Earth, 2003]. The detection and cataloging of these NEOs can help to identify those that may cross Earth's orbit and allow time for deflection of the NEO or other attempts to mitigate its impact. This threat caused the U. S. Congress to pass a mandate for detection of NEOs over 140 m in diameter [Near-Earth, 2003].

The current issue is how to detect those NEOs under 1 km in diameter but larger than 140 m. While current detection techniques can detect and catalogue 90 percent of the NEOs over 1 km in diameter, detecting those between 140 m and 1 km pose a more difficult task. New techniques need to be used to address this issue. The purpose of this thesis is to propose one such technique that may help bridge the gap so that 90 percent of NEOs over 140 m in diameter may be detected and catalogued for our safety.

Summation of Results and Findings

The process of using Nyquist sampling for data collection in the search for NEOs and measuring the atmospheric turbulence to create a PSF for a NEO at the visual magnitude limit of the telescope apparatus for the purposes of the cross-correlation increases the detection probability of NEOs at that visual magnitude limit. The Nyquist sampling rate reduces the spatial variance of the PSF within the CCD pixel FOV which allows for the use of cross-correlation to reduce the background noise. This process

improves the probability of detection for the NEO in the center of the pixel FOV by 129 percent. The process is most beneficial when the NEO is located in the corner of the pixel FOV and provides an improvement from 0 percent to 28 percent probability of detection.

Possible Follow-on Theses

Using this process on actual telescope data is the next step in validating it. This can be accomplished by recording images with Nyquist sampling and using this process to detecting known NEOs. The same data can be binned to form a Rayleigh sampling image that is then used in a threshold detector to detect the same NEOs and compare the results of the two processes for detection probabilities.

Appendix A – Nyquist Cross-Correlation MatLab Code

```
%MagnitudeTest.m
%2008/8/27
%Anthony O'Dell
%This program calculates the number of photons from a point source of a particular magnitude, creates a CCD image from a ground-based telescope, and uses either Nyquist sampling with cross-correlation of a PSF or Rayleigh sampling to measure its probability of detection. A threshold value (SNR) as a function of background standard deviations is used.
clear all;
clc;

format long;
load Constants;

%Flags
Corr = 1; % 1 means correlation with psf will be done, any other value and correlation with psf will not take place
Nyquist = 1; % 1 means Nyquist sampling will be used, otherwise, NEO report sampling will be used
Corner = 0; % 1 means NEO is in corner of pixel, else the NEO is in the center of the pixel
```

```
fid = fopen('NewNyquistCorrCenterSeeing10-20.txt', 'a');


%Inputs
for seeing = 10:20
dx_seeing = 14; % seeing used in aperture resolution
%seeing = 14; % in cm (atmopheric seeing parameter which causes psf), low
%value (1) bad, high value (20) great; for debugging purposes
n = 1000; %number of images
l = n/2; %number of bins and must be an integer
tau = 6; %given a normalized gaussian, tau is the number of standard
%deviations from the mean so as the reduce the number of false alarms
eta = .66; %quantum efficiency value from NEO report .66
%ccd must be kept square for psf function m x m matrix
ccd_x = 128; %number of pixels along x-axis of ccd
ccd_y = 128; %number of pixels along y-axis of ccd
telescope_radius = .5; %meters
vis_mag = 20.7;


if (Nyquist ==1)
    dx = 2*dx_seeing/ccd_y; %nyquist sampling
    integration_time = 1; %seconds
    background_mag = 21.4; %27 to 25 magnitude per square arcsec
```

```
else
    dx = 2*dx_seeing/(ccd_y*2.44); %NEO report sampling
    integration_time = 1; %seconds
    background_mag = 19.5; %27 to 25 magnitude per square arcsec
end

Vega_radius = 2.5*696000000; %meters
Vega_T = 9602; %Kelvin
Vega_Area = 4*pi*Vega_radius^2; %square meters
%Visible Power Emitted by the Vega; Vega is a blackbody radiater with a Gaussian
distribution
sigma = (10000/0.7):1:(10000/0.4); %Wave numbers; Important to note that delta
wavenumber is 1 cm
Luminosity = blackbody(sigma, Vega_T); %Watts/m^2 cm^-1 sr
VegaEarth_D = 25.3*9.461*10^15; %meters, distance from Earth to Vega
D_Area = 4*pi*VegaEarth_D^2; %meters^2; Surface area of Vega-centered sphere at
Earth distance
Power = Luminosity.*Vega_Area*4*pi/D_Area; %Watts
Incident_Power = Power/(2.512^vis_mag); %Watts/m^2
Background_Power = Power/(2.512^background_mag); %Watts/m^2

Aperature_Area = pi*(telescope_radius^2);%meters^2 area of telescope
```

```
Aperature_Power = Incident_Power*Aperature_Area; %Watts, Power incident on
telescope
ApBackground = Background_Power*Aperature_Area; %Watts, Power incident on
telescope
%background = 1344*integration_time*Aperature_Area; %night time background
photons per pixel (1e5); for daytime (1e7) for 128x128 ccd for 100 cm diameter telescope

Inverse_Photon_Energy = c*h*100*sigma; %Inverse energy per photon; 100 needed to
convert cm to meters
Wave_Length = length(sigma);

for i = 1:Wave_Length
   Photons(i) = eta*Aperature_Power(i)/Inverse_Photon_Energy(i);
   Background_Photons(i) = eta*ApBackground(i)/Inverse_Photon_Energy(i);
end
background = sum(Background_Photons)*integration_time;

%create psf source image without background noise
source_img=zeros(ccd_x,ccd_y);
source_img(ccd_x/2,ccd_y/2)=sum(Photons)*integration_time;
otf_long = Make_long_otf(telescope_radius*100, dx, ccd_y, seeing); %100 is used to
convert meters to centimeters
psf = fftshift(real(ifft2(fftshift(otf_long)))); %normalize point spread funtion
```

```
if (Corner == 1)
   psf_source = makeshift(psf*source_img(ccd_x/2,ccd_y/2),.5,.5);
else
   psf_source = psf*source_img(ccd_x/2,ccd_y/2);
end
%figure(2); imagesc(psf_source);

%create background and source images
for i = 1:n
   source(:,:,i) = poissrnd(psf_source+background, ccd_x, ccd_y);
   background_noise(:,:,i) = poissrnd(ones(ccd_x,ccd_y)*background);
   if (Corr == 1)
%Subtract off background from images
      source_subtract(:,:,i) = source(:,:,i)-background;
      background_subtract(:,:,i) = background_noise(:,:,i)-background;
% Cross-correlate the image with the psf by taking the fft of both and multiplying the
two, then taking the inverse fft and only the real part
      noise_source(:,:,i) = real(ifft2(fft2(fftshift(psf)).*conj(fft2(source_subtract(:,:,i)))));
      noise_background(:,:,i) =
real(ifft2(fft2(fftshift(psf)).*conj(fft2(background_subtract(:,:,i)))));
   else
%Subtract off background from images
      noise_source(:,:,i) = source(:,:,i)-background;
```

```
        noise_background(:,:,i) = background_noise(:,:,i)-background;
    end
%Find means
    source_mean(i) = sum(sum(noise_source(:,:,i)))/(ccd_x*ccd_y);
    background_mean(i) = sum(sum(noise_background(:,:,i)))/(ccd_x*ccd_y);
%Find standard deviations
    source_stan_dev(i) = sqrt(sum(sum(((noise_source(:,:,i)-
source_mean(i)).^2)))/(ccd_x*ccd_y));
    background_stan_dev(i) = sqrt(sum(sum(((noise_background(:,:,i)-
background_mean(i)).^2)))/(ccd_x*ccd_y));
end

%Calculate average standard deviation and use it find threshold for detection
stan_dev_b = sum(background_stan_dev)/n;
%false_alarms_theory = ccd_x*ccd_y*n*threshold(tau);
threshold = stan_dev_b*tau;

for i=1:n
    binmap(:,:,i)=(noise_source(:,:,i)>threshold);
    binmap_back(:,:,i)=(noise_background(:,:,i)>threshold);
end
%Use threshold detector to find positive and false hits in images
pd(seeing) = 0;
```

```
pfa(seeing) = 0;
pfa(seeing) = sum(sum(sum(binmap_back)))/(ccd_x*ccd_y*(n-1));
if (Corner == 1)
%    pfa(seeing) = (sum(sum(sum(binmap)))-sum(binmap(65,65,:))-
sum(binmap(66,65,:))-sum(binmap(65,66,:))-sum(binmap(66,66,:)))/(ccd_x*ccd_y*(n-
1));
   for i=1:n
      if ((binmap(65,65,i)+binmap(66,65,i)+binmap(65,66,i)+binmap(66,66,i)) > 0)
      pd(seeing) = pd(seeing)+(1/n);
      end
   end
else
%    pfa(seeing) = (sum(sum(sum(binmap)))-sum(binmap(65,65,:)))/(ccd_x*ccd_y*(n-
1));
   pd(seeing) = sum(binmap(65,65,:))/n;
end
%write data to file
printing = fprintf(fid, '%5g %5g %5g\n', seeing, pfa(seeing), pd(seeing));
end
status = fclose(fid);
```

Bibliography

Catalina Sky Survey. http://www.lpl.arizona.edu/css/. 2008.

Chelsey, Steve and others. "Asteroid 2008 TC3 Strikes Earth: Predictions and Observations Agree." http://www.spaceguarduk.com/centre/news/3-latest-news/42-2008-tc3. 5 November 2008.

Evans, J. B. and others. "Detection and Discovery of Near-Earth Asteroids by the LINEAR Program," *Lincoln Laboratory Journal*, Vol. 14, No. 2, pp. 199–220, 2003.

Fix, John D. *Astronomy: Journey to the Cosmic Frontier*. Mosby-Year Book, Inc., 1995.

Goodman, Joseph W. *Goodman Statistical Optics*. John Wiley & Sons, Inc., 2000.

Kirchner, George and others. "Measuring Atmospheric Seeing with kHz SLR." http://cddis.gsfc.nasa.gov/lw15/docs/papers/Measuring%20Atmospheric%20Seeing%20with%20KHz%20SLR.pdf.

Lahti, B. P. *Signal Processing and Linear Systems*. Berkeley Cambridge Press, 1998.

Lincoln Laboratory, Massachusetts Institute of Technology. http://www.ll.mit.edu/mission/space/linear/. 2008.

NASA Jet Propulsion Laboratory. http://neo.jpl.nasa.gov/stats/. 2008.

Near-Earth Object Science Definition Team. *Study to Determine the Feasibility of Extending the Search for Near-Earth Objects to Smaller Limiting Diameters.* 22 August 2003.

Yeomans, Don. "Small Asteroid Predicted to Cause Brilliant Fireball Over Southern Sudan." http://neo.jpl.nasa.gov/news/news159.html. 6 October 2008.

Yeomans, Don. "Impact of Asteroid 2008 TC3 Confirmed." http://www.lpl.arizona.edu/css/2008TC3_2.html. 7 October 2008.

Young, Hugh D. *Statistical Treatment of Experimental Data*. McGraw-Hill Book Company, Inc., 1962.

Vita

Captain Anthony O'Dell graduated from the University of Oklahoma in Norman, OK in 2000 with a B.S. in Astrophysics. He entered the USAF in 2004 and received a Graduate Certificate in Measurement and Signatures Intelligence from the Air Force Institute of Technology in 2005.

REPORT DOCUMENTATION PAGE

Form Approved
OMB No. 074-0188

1. REPORT DATE *(DD-MM-YYYY)*	2. REPORT TYPE	3. DATES COVERED *(From – To)*
26-03-2009	**Master's Thesis**	May 2007 – Mar 2009

4. TITLE AND SUBTITLE

Detecting Near-Earth Objects Using Cross-Correlation with a Point Spread Function

5a. CONTRACT NUMBER

5b. GRANT NUMBER

5c. PROGRAM ELEMENT NUMBER

6. AUTHOR(S)

O'Dell, Anthony, P., Captain, USAF

5d. PROJECT NUMBER
N/A

5e. TASK NUMBER

5f. WORK UNIT NUMBER

7. PERFORMING ORGANIZATION NAMES(S) AND ADDRESS(S)

Air Force Institute of Technology
Graduate School of Engineering and Management (AFIT/EN)
2950 Hobson Way, Building 640
WPAFB OH 45433-8865

8. PERFORMING ORGANIZATION REPORT NUMBER

AFIT/GE/ENG/09-30

9. SPONSORING/MONITORING AGENCY NAME(S) AND ADDRESS(ES)

Air Force Research Laboratory
Attn: Maj. David M. Strong, PhD.
535 Lipoa Pkwy, Suite 200 Phone: (808) 891-7753
Kihei HI 96753 e-mail: David.Strong@maui.afmc.af.mil

10. SPONSOR/MONITOR'S ACRONYM(S)
AFRL/RDSM

11. SPONSOR/MONITOR'S REPORT NUMBER(S)

12. DISTRIBUTION/AVAILABILITY STATEMENT

APPROVED FOR PUBLIC RELEASE; DISTRIBUTION UNLIMITED.

13. SUPPLEMENTARY NOTES

14. ABSTRACT

This thesis describes a process to help discover Near-Earth Objects (NEOs) of larger than 140 meters in diameter from ground based telescopes. The process involves using Nyquist sampling rate to take data from a ground-based telescope and measuring the atmospheric seeing parameter, r_0, at the time of data collection. r_0 is then used to create a point spread function (PSF) for a NEO at the visual magnitude limit of the telescope and exposure time. This PSF is cross-correlated with the Nyquist sampling rate image from the telescope to reduce the noise and therefore increase the detection probability of a faint NEO. The process is compared to the current detection technique of using Rayleigh sampling with a threshold detector. This process is tested versus improper seeing parameter measurement and different locations of the NEO within the charged-coupled device (CCD) pixel field of view (FOV). The biggest improvement is where the NEO is located in the corner of the pixel FOV. The new process shows improvement in detection probability over the current process in all simulations.

15. SUBJECT TERMS

Near-Earth objects, asteroids, cross-correlation, matched filter, detection.

16. SECURITY CLASSIFICATION OF:			17. LIMITATION OF ABSTRACT	18. NUMBER OF PAGES	19a. NAME OF RESPONSIBLE PERSON
a. REPORT	b. ABSTRACT	c. THIS PAGE			Dr. Stephen C. Cain, USAF (ENG)
U	U	U	UU	60	**19b. TELEPHONE NUMBER** *(Include area code)* (937) 255-3636, ext 4617; e-mail: Stephen.Cain@afit.edu

Standard Form 298 (Rev. 8-98)
Prescribed by ANSI Std. Z39-18